ELSEVIER

Journal of Structural Geology 27 (2005) 1803–1822

JOURNAL OF STRUCTURAL GEOLOGY

www.elsevier.com/locate/jsg

Controls on damage zone asymmetry of a normal fault zone: outcrop analyses of a segment of the Moab fault, SE Utah

Silje S. Berg*, Tore Skar

Centre for Integrated Petroleum Research, University of Bergen, Allégt. 41, 5007 Bergen, Norway

Received 25 May 2004; received in revised form 18 October 2004; accepted 20 April 2005
Available online 1 August 2005

Abstract

Outcrop data has been used to examine the spatial arrangement of fractures in the damage zones of a segment of the large-scale Moab Fault (45 km in length), SE Utah. The characteristics of the footwall and hanging wall damage zones show pronounced differences in the deformation pattern: (1) there is a well-developed syncline in the hanging wall, as opposed to sub-horizontal bedding of the footwall; (2) the footwall damage zone is sub-divided into an inner zone (0–5 m from fault core) and an outer zone (>5 m) based on differences in deformation band frequency, whereas no clear sub-division can be made in the hanging wall; (3) the hanging wall damage zone is more than three times wider than the footwall damage zone; (4) there is a higher abundance of antithetic fractures and deformation bands in the hanging wall than in the footwall; and (5) the antithetic structures generally have more gentle dips in the hanging wall than in the footwall. The main conclusion is that the structural pattern across the fault zone is strongly asymmetric. The deformation pattern is partly influenced by lithology and/or partly by processes associated with the development of the fault core. We suggest, however, that the most important cause for the asymmetric strain distribution is the development of the hanging wall syncline and the resulting asymmetric stress pattern expected to exist during fault propagation.

Keywords: Normal fault; Fault zone architecture; Damage zone; Deformation band

1. Introduction

Fault zones may have important implications for fluid flow in the earth's shallow crust as they commonly act as localized conduits or barriers (McCaig, 1988; Sibson, 1992, 1994, 1996; Sibson and Scott, 1998) because the permeability of fault zones may be several orders of magnitude higher or lower than the host rock (Pittman, 1981; Antonellini and Aydin, 1994; Evans et al., 1997; Seront et al., 1998; Zhang and Tullis, 1998). The petrophysical properties are controlled by the fault zone architecture and the intrinsic properties of fault-related rocks (Smith et al., 1990; Bruhn et al., 1994; Caine et al., 1996; Evans et al., 1997; Gibson, 1998; Rawling et al., 2001; Shipton et al., 2002). The fault zone architecture is commonly complex, depending on the history of faulting (temperature, pressure, stress conditions, strain rate) (Heermance et al., 2003) and lithology (Mandl, 2000), and may vary spatially and temporarily along the same fault zone (Smith et al., 1990; Bruhn et al., 1994).

Faults are commonly described as zones consisting of a fault core and a surrounding damage zone, which differs structurally, mechanically and petrophysically from the undeformed host rock (protolith) (Chester and Logan, 1986; Smith et al., 1990; Forster and Evans, 1991; Chester et al., 1993; Bruhn et al., 1994; Caine et al., 1996). The *fault core* represents the part of the fault zone where most of the displacement is accommodated. It consists of various structures, including slip surfaces, gouge, breccias, cataclasites, clay smears, horses, and geochemically altered rock bodies (Chester and Logan, 1986; Chester et al., 1993; Bruhn et al., 1994; Caine et al., 1996; Clausen, 2002; Clausen et al., 2003). The *damage zone* is the deformed rock volume that surrounds the fault core, and may be comprised of subsidiary faults, fault rocks, veins, joints, stylolites, cleavage and folds (Chester and Logan, 1986, 1987; Wu and

* Corresponding author. Present address: Statoil Research Center, Rotvoll, Arkitekt Ebellsvei 10, 7005 Trondheim, Norway. Tel.: +47 99579172; fax: +47 73967286.
E-mail address: silje.berg@statoil.com (S.S. Berg).

0191-8141/$ - see front matter © 2005 Elsevier Ltd. All rights reserved.
doi:10.1016/j.jsg.2005.04.012

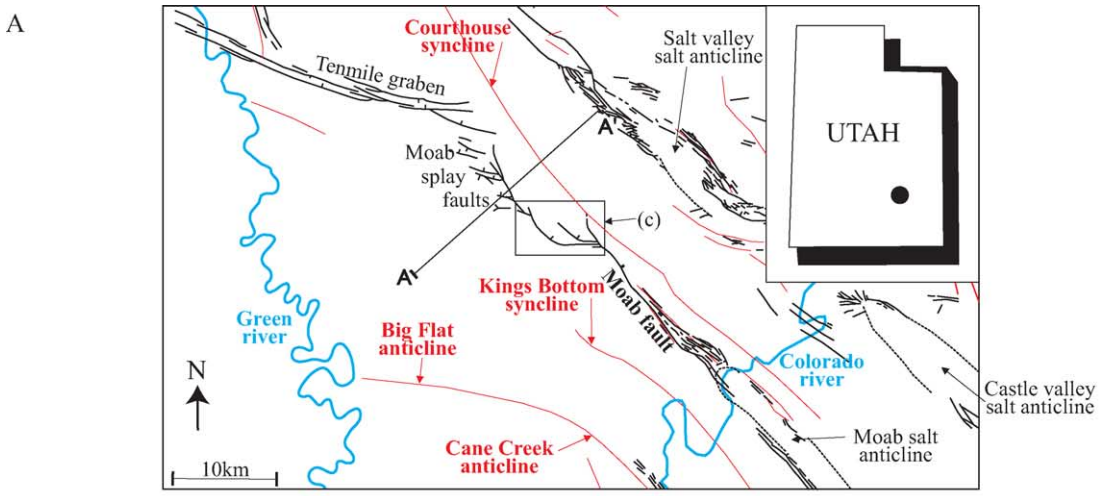

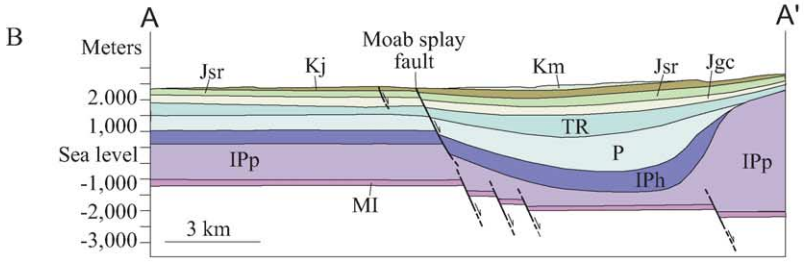

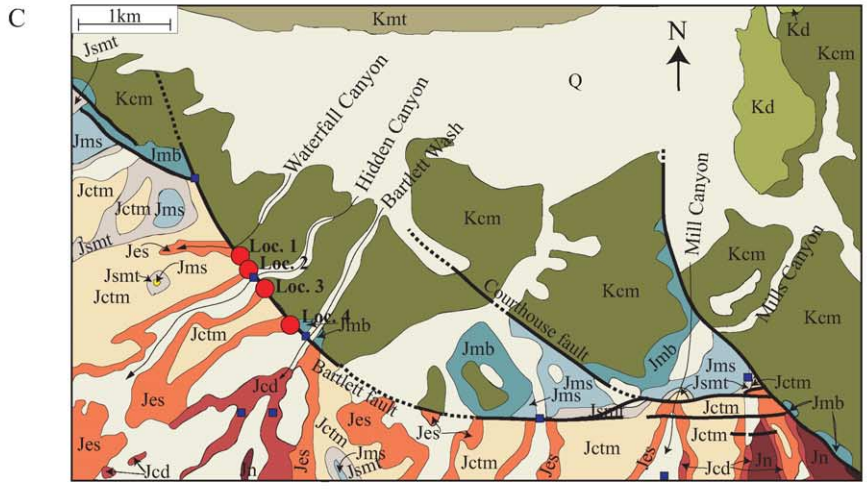

Q Quaternary eolian and alluvial deposits
Kmt Tununk Shale Mb of Mancos Shale
Kd Dakota Sst
Kcm Cedar mountain Fm
Jmb Brushy Basin of Morrison Fm
Jms Salt Wash Mb of Morrison Fm
Jsmt Tidwell Mb of Morrison Fm/ Summerville Fm undivided
Jctm Moab Mb of Curtis Fm
Jes Slick Rock Mb of Entrada Sst
Jcd Dewey Bridge Mb of Carmel Fm
Jn Navajo Sst
Jk Kayenta Fm
Localities
Spring

D

Period	Formation		
Cretaceous			
	Dakota Sst		KJ i (b) = Cedar Mountain/ Burro Canyon/ Morrison Fms undivided)
	Cedar Mountain Fm		
Jurassic	Morrison Fm		
	Jsr San Rafael Group	**Curtis Fm**	**Moab Mb**
		Entrada Sst	**Slick Rock Mb**
		Carmel Fm	Dewey Bridge
	Jgc Glenn Canyon Group	Navajo Sst	
		Kayenta Fm	
		Wingate	
TR Triassic	Chinle Fm		
	Moenkopi Fm		
P Permian	Cutler Fm		
Carboniferous	IPh Honaker Trail		
	IPp Paradox Fm		
	MI Leadville Fm		

Fig. 1. (a) Overview map showing the main structures in the area around Moab, Utah. (b) Cross-section through the northwestern segment of the Moab fault. Location of the cross-section is indicated in (a), abbreviations for units are shown in (d). (c) Geological map of the study area, with localities marked in red. (d) Stratigraphic units that are cut by the Moab fault. The lithological units hosting the Bartlett fault segment at the studied outcrops are marked with bold letters. The Moab Member was previously a member of the Entrada Sandstone, but were reclassified by Doelling (2001). Modified from Doelling (2001) and Foxford et al. (1996, 1998). Springs in (c) are inferred from topographic maps (United States Geological Survey, 1985, 1988).

Groshong, 1991; Chester et al., 1993; Bruhn et al., 1994; Caine et al., 1996; Hesthammer et al., 2000; Jourde et al., 2002). The damage zone is also commonly affected by geochemical and mineralogical alteration (Schulz and Evans, 1998, 2000, and references therein).

Although this conceptual fault zone model has been widely accepted, extensions of the model, with a further subdivision of the fault zone components, have been proposed (Gabrielsen and Aarland, 1990; Jones and Knipe, 1996; Braathen and Gabrielsen, 1998; Heynekamp et al., 1999; Clausen et al., 2003; Kim et al., 2004). These extensions applies to different geological settings, and include (1) a general subdivision into five zones (A–E) based on fracture frequency and presence of fault rocks and cements in crystalline rocks (Braathen and Gabrielsen, 1998), (2) subdivisions of the fault core into central and distal parts (Clausen et al., 2003) or core zone and mixed zones (Heynekamp et al., 1999) based on continuity of clay membranes in poorly lithified sediments, (3) subdivisions of the damage zone into inner and outer regions based on strain distribution (Jones and Knipe, 1996; Micarelli et al., 2003) or tip-, wall-, and linking zones according to the location around the faults (Kim et al., 2004), and finally (4) subdivision of zones within deformation bands in porous sandstones based on differences in compaction, grain reorientation and size-reduction, mineralization, and jointing (Gabrielsen and Aarland, 1990).

It is also shown that inclined faults commonly display an asymmetric deformation pattern around the fault core (Aydin and Johnson, 1978; Antonellini and Aydin, 1995; Nelson et al., 1999; Mitra and Ismat, 2001; Clausen et al., 2003; Doughty, 2003). This asymmetry may be related to irregularities on the fault trace (Gabrielsen et al., 1998; Aarland and Skjerven, 1998), to different stress conditions in the footwall and hanging wall during faulting (Mandl, 1988, 2000; Knott et al., 1996), and/or to differences in rock properties across the fault. In this paper, we examine whether this revised model of damage zone asymmetry are applicable to a segment of a regional normal fault in siliclastic rocks. We then consider relevant factors that may contribute to the asymmetric strain distribution, and evaluate possible mechanisms responsible for the observed deformation pattern. A segment of the Moab Fault Zone, SE Utah, was selected for this purpose because the footwall and hanging wall damage zones are well exposed, allowing for comparison of damage zone characteristics.

2. Geological setting

The Moab Fault is a 45 km long normal fault in the northeastern part of the Paradox Basin, SE Utah (Fig. 1a) (Foxford et al., 1996). The fault affects a ca. 5000-m-thick sedimentary sequence of Carboniferous to Cretaceous age (Fig. 1b). It has an estimated maximum dip-slip displacement of 950 m in surface exposures, increasing to nearly 1800 m in the deeply buried Pennsylvanian sequence (Foxford et al., 1996). Activity on the fault was related to either (1) Mesozoic to Cenozoic regional extension that promoted salt movement, (2) subsidence due to dissolution of salt below the clastic strata of the Moab salt-anticline, (3) Tertiary extension and reactivation of basement faults due to relaxation of the Laramide Orogeny, or (4) Late Tertiary, thin-skinned extension (Olig et al., 1996 and references therein). Foxford et al. (1996) suggest that the fault was active during two main episodes; from the Triassic to pre-middle Jurassic and from Early Cretaceous until Early Tertiary. Summary diagrams for geologic events and their timing are compiled by Garden et al. (2001) and Davatzes and Aydin (2003).

Several normal faults are associated with the salt-anticlines in the Moab region (Fig. 1a) (Doelling, 2001). In the southeast, the Moab fault strikes parallel to the Moab anticline (NW–SE), and continues farther northwestwards along the Courthouse syncline, where it eventually dies out. At its northwestern tip, several footwall fault segments splay from the main fault trace. These segments curve and become parallel with the main fault trace several kilometers west of their branching points (Fig. 1a). The northwestern extension of the fault may be linked to the Tenmile graben, and in the southeast, the displacement is accommodated along the Lisbon fault (Foxford et al., 1996). One of the splaying segments of the Moab fault, commonly referred to as the Bartlett fault (Koestler et al., 1994), is the focus of this paper. The estimated normal throw at the studied localities is between 170 and 300 m (Foxford et al., 1996).

The rock units in the study area have been thoroughly described by Doelling (2001). Exposed footwall host rock consists of Jurassic eolian sandstones, belonging to the Slick Rock Member of the Entrada Sandstone and the Moab Member of the Curtis Formation, recently reassigned by Doelling (2001) (Fig. 1c and d). The ca. 60-m-thick Slick Rock Member Sandstone is orange-red, generally medium- to fine-grained, and cross-bedded to massive. It consists of ca. 95% quartz and minor occurrences of alkali feldspar, and secondary hydrated iron oxide and calcite cement. At the studied localities, the thickness of the Moab Member is around 23 m. The Moab Member is a pale-yellow to gray, fine- to medium-grained sandstone, and is cross-bedded to massive. Apart from a 40-cm-thick layer of mudstone in the lower section, the Moab Member sandstone contains less fine-grained material and is better sorted than the Slick-Rock Member. It is also a quartz sandstone, consisting of ca. 98% quartz grains and minor occurrences of alkali feldspar. Secondary minerals are present mainly as quartz cement and there is some hydrated iron oxide.

The exposed lithology of the hanging wall is heterogeneous, consisting of various fluvial sandstones and conglomerates that belong to the Cretaceous Cedar Mountain Formation (Doelling, 2001). The exposed thickness of this formation varies between 2 and 7 m. The

analyzed section is sub-divided into five major units: (1) medium grained, moderately cemented sandstone, (2) intercalated moderately and highly cemented sandstone, (3) conglomerate, (4) moderately cemented, fine to coarse-grained sandstone with lenticular beds of highly cemented, fine-grained sandstone, and (5) massive fine- and medium-grained sandstone, which is cemented to varying degrees. Thus, the heterogeneity of the rock is defined by variations in texture (e.g. grain sizes, sorting) and degree of cementation. The Cedar Mountain Formation rests on the underlying Brushy Basin Member of the Morrison Formation (Doelling, 2001). Brushy Basin Member is expected to have influenced the development of the hanging wall damage zone as is consists of mudstone and may have had distinctively different mechanical properties than the exposed rocks of the Cedar Mountain Formation at the time of faulting.

3. Methods

The Bartlett fault segment of the Moab fault is well exposed in several canyons that are oriented perpendicular to the strike of the fault. Outcrops in three of the canyons were studied in detail (localities 1–4; Fig. 1c). The data used in this analysis were obtained directly from outcrop study by use of conventional structural techniques, digital imaging, fracture trace mapping, and scan-line methods. The scan lines were 50–70 m long, and oriented parallel to sub-horizontal bedding of the footwall and perpendicular to the fault zone. All lines start at the margin of the fault core, and cover the footwall damage zone and parts of the unaffected protolith. Due to the heterogeneous character of the hanging wall rocks, continuous traverses in the hanging wall damage zone were difficult to obtain. Therefore, short fracture traverses were used to gather data from individual lithological/mechanical units.

The data recorded from traverses in the footwall include fracture type, frequency, orientation, geometry, and termination (Table 1). The *fracture termination* is described based on five categories: (i) both ends free, (ii) one end connected, (iii) both ends connected, (iv) splayed ends, and (v) unknown. These give an indication of the fracture connectedness. In general, the present description follows the nomenclature of Peacock et al. (2000). We define *fractures* as planar to semi-planar discontinuities caused by stress. These include joints, deformation bands, and slip surfaces. The term *joint* is used for discrete fractures without apparent shear displacement, but which constitute discontinuities in the rock mass (Pollard and Aydin, 1988). *Deformation bands* are small faults (mm to a few cm displacements) characterized by a zone of pore collapse and grain fracturing and with no discrete surface of discontinuity (Aydin, 1978). *Slip surfaces* are discrete through-going surfaces with displacements up to several meters (Aydin and Johnson, 1978).

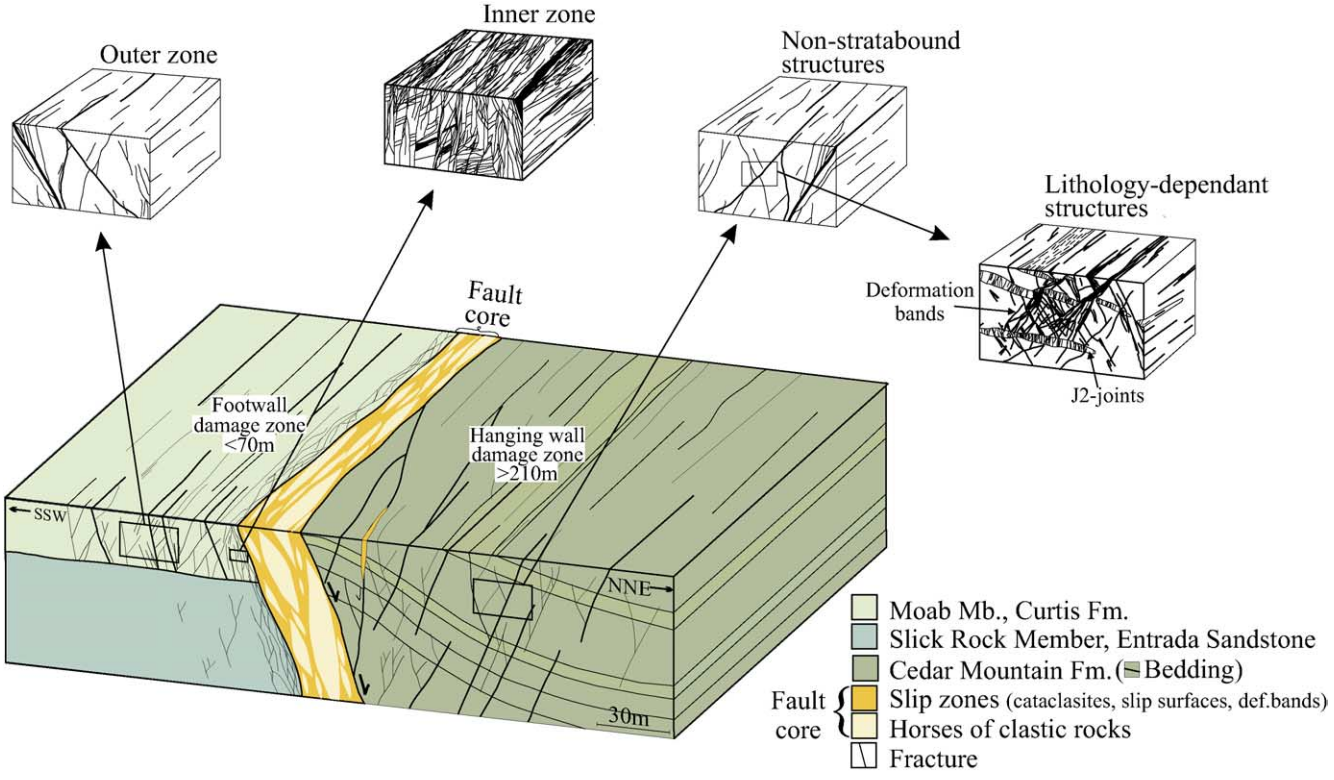

Fig. 2. Overview of the main architectural components of the Bartlett fault.

Table 1
Data obtained from traverses

Parameters	Description
Fracture type	Joint vs. shear fracture Deformation band vs. discrete fracture Vein vs. non-mineralized fracture
Fracture frequency	Number of fractures (*N*) per meter
Orientation	Strike and dip, slip orientation where available
Geometry	Planar, slightly undulating, undulating, or curved
Fracture termination	Both ends free, one end connected, both ends connected, splayed ends, or unknown

4. Fault zone architecture

The Bartlett fault consists of a fault core surrounded by damage zones in the footwall and hanging wall (Fig. 2). The fault core is structurally complex and lithologically heterogeneous. It consists of a variety of fault rocks and entrained bodies of clastic host rocks (horses) (Fig. 3a) that indicate considerable variation in strain intensity and deformation style. The internal characteristics lead to a locally irregular geometry at the margins of the fault core (Fig. 3b). These irregularities may have implications for the characteristics in the damage zones.

In contrast to the fault core, the damage zones are characterized by relatively weakly deformed bedrock. Both damage zones contain three dominant types of discontinuities, namely deformation bands, slip surfaces, and joints. Commonly, deformation bands show displacements in the range of few centimeters. They occur as single strands (Aydin, 1978), in zones (Aydin and Johnson, 1978), or as clusters (Shipton and Cowie, 2001). The slip surfaces have displacements in the order of a few millimeters to up to a meter, and have planar to slightly curved geometry. All these fracture types typically strike subparallel to the fault; however, the relative distribution of synthetic and antithetic fractures, the dip angle of the fractures, and the fracture distribution are somewhat different across the foot- and hanging wall damage zones.

The hanging wall damage zone is characterized by a more than 210-m-wide, fault-parallel syncline (Fig. 2). It displays a more complex rock-, fracture- and cementation-pattern than the footwall damage zone where the bedding of eolian sandstone is sub-horizontal. The differences in lithology between the hanging wall and footwall are expected to influence the strain characteristics within the damage zones. Yet, there are indications that factors other than lithology control differences in deformation between the hanging wall and footwall. In the following sections, each of the damage zones will be described in detail, with emphasis on the structural variation.

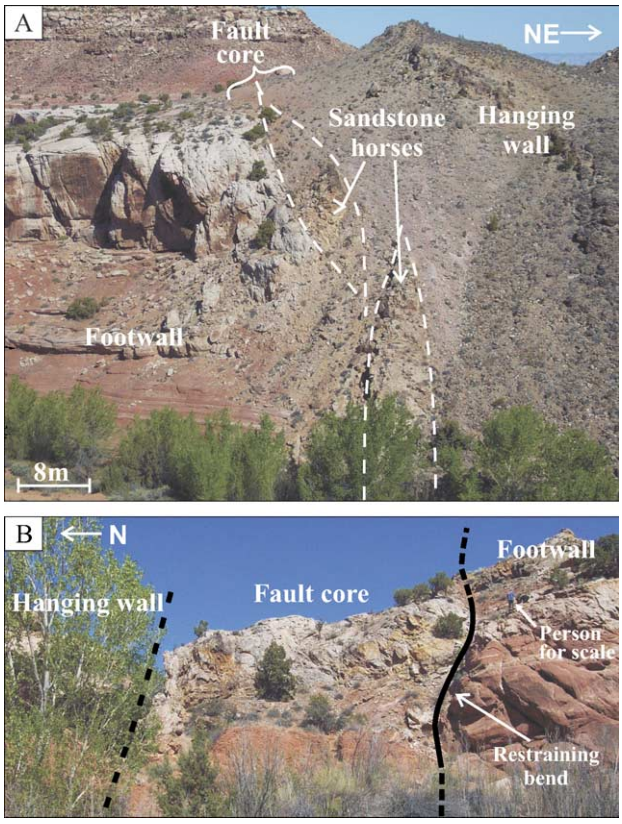

Fig. 3. (a) Overview of the Bartlett fault at Hidden Canyon showing elongate rock bodies (horses) present in the fault core. (b) Irregular geometry at the fault core margin exposed in Tusher Canyon.

4.1. Footwall damage zone

4.1.1. Fracture types

Deformation bands constitute the most common structure in the footwall damage zone. Slip surfaces and joints occur more locally. The deformation bands are dominantly WNW–ESE-trending and steeply dipping (ca. 85°) (Fig. 4), with a slight predominance of antithetic (SSW-dipping) structures (55%). The latter structures reveal a greater variation in dip than the synthetic bands. Geometries vary

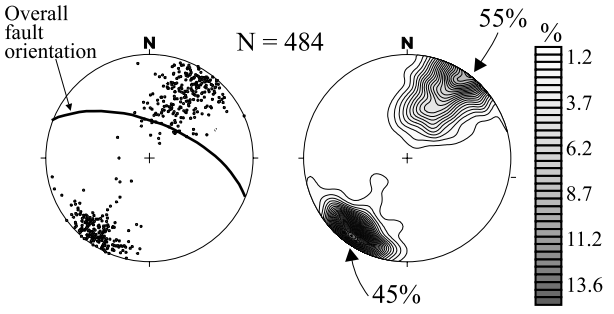

Fig. 4. Stereo-plots of deformation bands in the footwall damage zone (Moab Mb), plotted as poles to planes and contoured poles to planes. Equal area, lower hemisphere stereo-net.

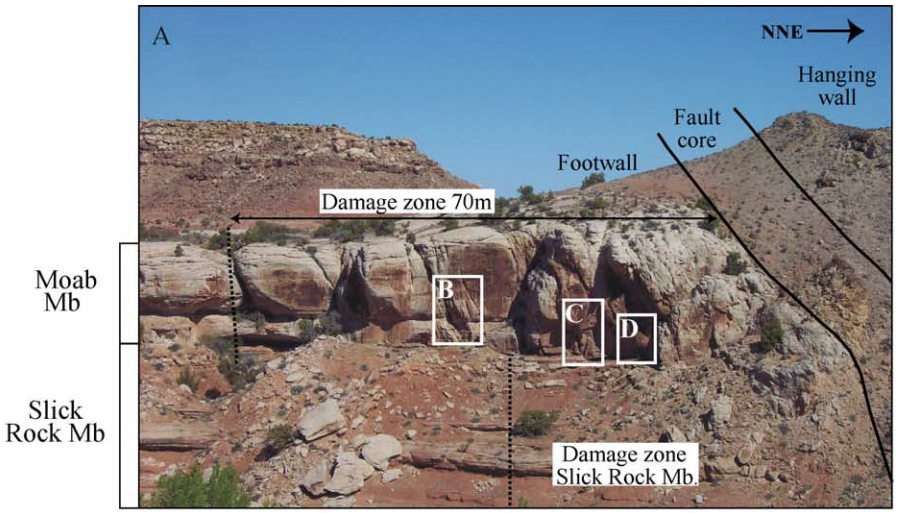
A
NNE
Hanging wall
Fault core
Footwall
Damage zone 70m
Moab Mb
Slick Rock Mb
B
C
D
Damage zone Slick Rock Mb.

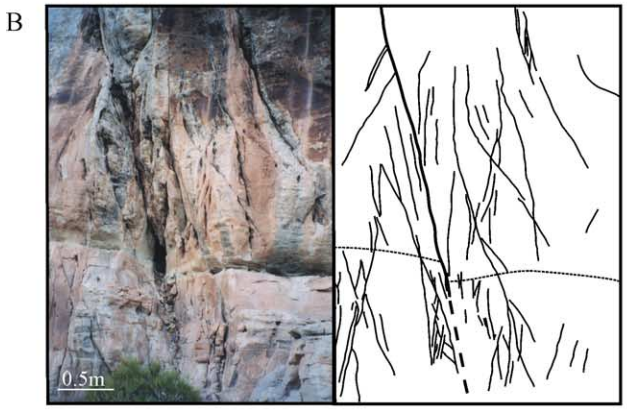
B
0.5m

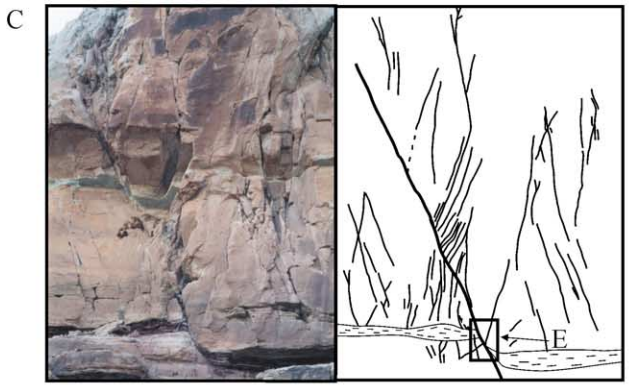
C
E

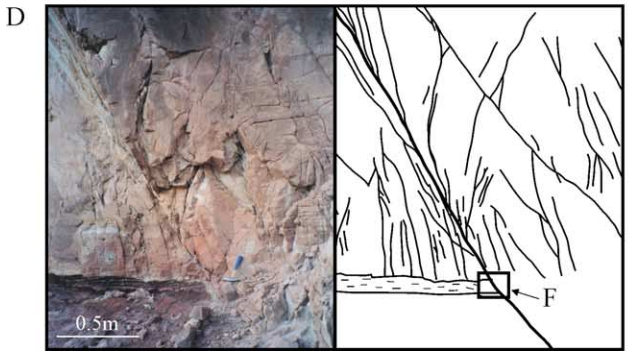
D
0.5m
F

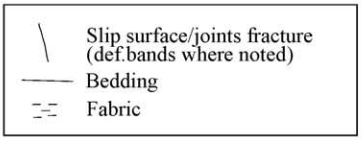
Slip surface/joints fracture (def.bands where noted)
Bedding
Fabric


E
15cm

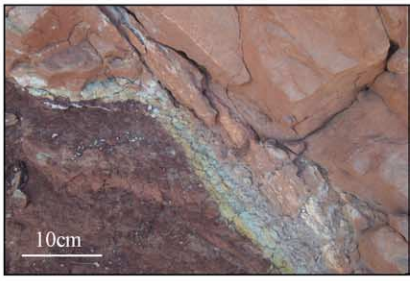
F
10cm

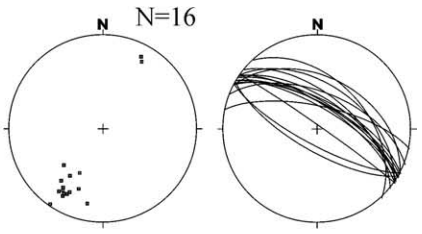
G
N=16
N
N

Table 2
Average frequency of deformation bands

		Moab Member, Canyon B (Fig. 6b)	Moab Member, Canyon B (Fig. 6c)	Slick Rock Member, Bartlett Wash (Fig. 6d)	Moab Member Hidden Canyon (Fig. 6e)
Footwall damage zone	Width (m)	36	40	43	58
	N	323	267	155	194
	N/width	**8.9**	**6.7**	**3.6**	**3.3**
Outer and transitional zones	Width (m)	31	35	39	58
	N	114	116	55	194
	N/width	**3.6**	**3.3**	**1.4**	**3.3**

from planar (21%), slightly undulating (46%), undulating (7%) to curved (26%). *Slip surfaces* dip between 44 and 87°, and appear both as synthetic and subordinately antithetic structures (Fig. 5a–d). Some clay smears are observed in association with a thin mudstone bed in lower parts of the Moab Member (Fig. 5e and f). *Joints* have planar geometries. They also have the same overall orientations as the synthetic and antithetic slip surfaces. There is no significant change in orientation for any of the fracture types with distance from the fault core, neither is there any systematic change in their geometry.

4.1.2. Spatial fracture distribution

Deformation bands appear either isolated from other fracture types, or they occur associated with slip surfaces and joints. In the latter case, they commonly form subsidiary fault zones (Fig. 5a–d), where minor synthetic and antithetic slip surfaces, deformation bands, and joints surround a central slip surface. Davatzes and Aydin (2003) demonstrate an age relationship between these structures, where the deformation bands are overprinted by the joints and subsequent slip and development of the slip surfaces. The subsidiary fault zones are dominantly synthetic to the master fault zone, and are most prominent in the Moab Member in areas more than 5 m from the fault core.

The total number of deformation bands measured along scan-lines ranges from 155 to 323 (Table 2), whereas slip surfaces and joints are sparse. The frequency varies between 0 and 55 deformation bands per meter, with the highest frequencies proximal to the fault core (Fig. 6). Based on the difference in deformation band frequency, the footwall damage zone may be divided into two sub-zones. The *inner zone* is defined by the high frequency (10–55 deformation bands per meter) found in the first 4–5 m of the footwall (Fig. 6b–d). This zone contains 55–65% of the total deformation bands measured along the scan-lines, and shows a near linear, high gradient cumulative frequency curve (Fig. 6a). The *outer zone* is defined by lower frequencies measured at distances exceeding about 5 m from the fault core. On average, the fracture frequency is eight times higher in the inner zone compared with that of the outer. Similar observations from the Bartlett fault are reported by Harris et al. (2003), who found that the 'inner damage zone' is from 5 to 10 m wide. However, at some localities the inner zone is absent (Fig. 6e), and the deformation band frequency never rises above 20 per meter.

The margin of the outer zone is located where the cumulative frequency curve shifts from being curved or semi-linear with a high gradient to become linear with a low gradient (Fig. 6a). The linear, low-gradient curve defines a transitional zone to the unaffected protolith. Fractures in the unaffected protolith represent a background fracture system characterized by a frequency in the range of 0.1–1 fractures per meter. The total width of the footwall damage zone (including the transitional zone) varies from 36, 40, and 58 m in the Moab Member to 43 m in the Slick Rock Member (Fig. 6b–e). If the outermost subsidiary fault zone is included, the damage zone is as wide as 70 m (Moab Member, locality 2). Other workers have reported damage zone widths in the range of 12 m (Koestler et al., 1995), 15–22 m (Davatzes and Aydin, 2003), 20–50 m (Koestler et al., 1994) and up to 60 m (Harris et al., 2003) along this same fault. Thus, it can be concluded that the footwall damage zone of the Bartlett fault has no constant width, but varies from one locality to the other along the strike of the fault.

Connectedness is inferred from observations of deformation band terminations (Table 1). In the inner zone, 92% of the deformation bands are connected at one or both ends, whereas 76% of the deformation bands in the outer zone are connected in a similar manner. Higher connectedness in the inner zone is well illustrated on fracture trace maps (Fig. 7).

By comparing the average deformation band frequencies between different localities, we find that the frequency decreases with increasing damage zone width (Table 2). The average frequency is 9, 7, 4, and 3 deformation bands per meter in areas where the footwall damage zone is 36, 40, 43,

Fig. 5. (a) Overview photograph from Hidden Canyon (locality 2), where the footwall damage zone is at its widest. (b)–(d) Enlarged sections that illustrate the architecture of subsidiary fault zones. These fault zones consist of a central slip surface and surrounding synthetic and antithetic discontinuities, including slip surfaces, deformation bans, and joints. Note that deformation bands are numerous and only a few are visible on photographs at this scale. (e) and (f) Enlarged sections of clay smears associated with the faults in (c) and (d), respectively. (g) Orientation data from two of the subsidiary faults (in (c) and (d)) showing a predominance of synthetic structures. Planes and poles to planes in equal area, lower hemisphere stereo-net.

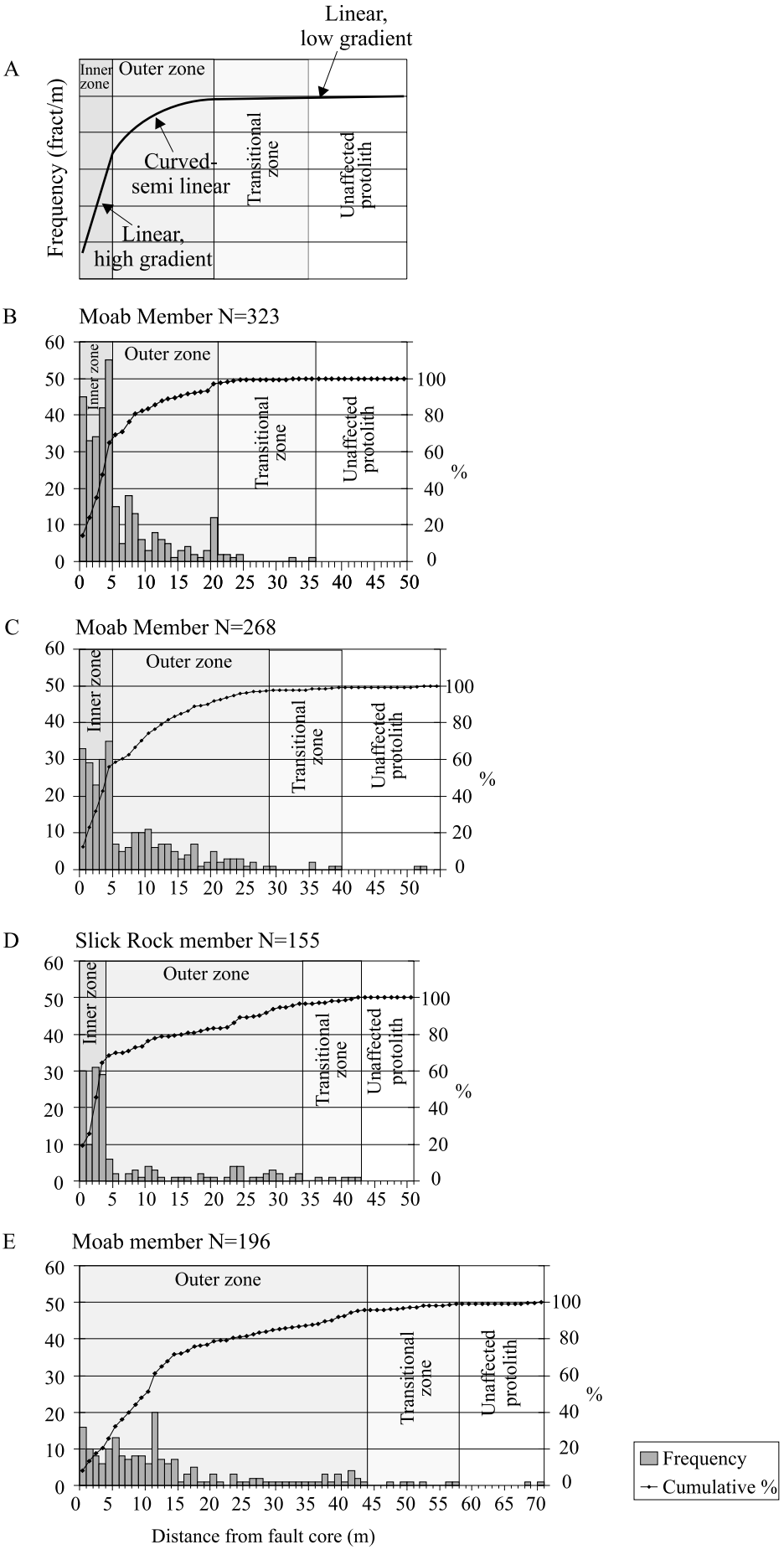
A
Linear, low gradient
Inner zone
Outer zone
Frequency (fract/m)
Curved-semi linear
Linear, high gradient
Transitional zone
Unaffected protolith
B
Moab Member N=323
C
Moab Member N=268
D
Slick Rock member N=155
E
Moab member N=196
Inner zone
Outer zone
Transitional zone
Unaffected protolith
%
Distance from fault core (m)
Frequency
Cumulative %

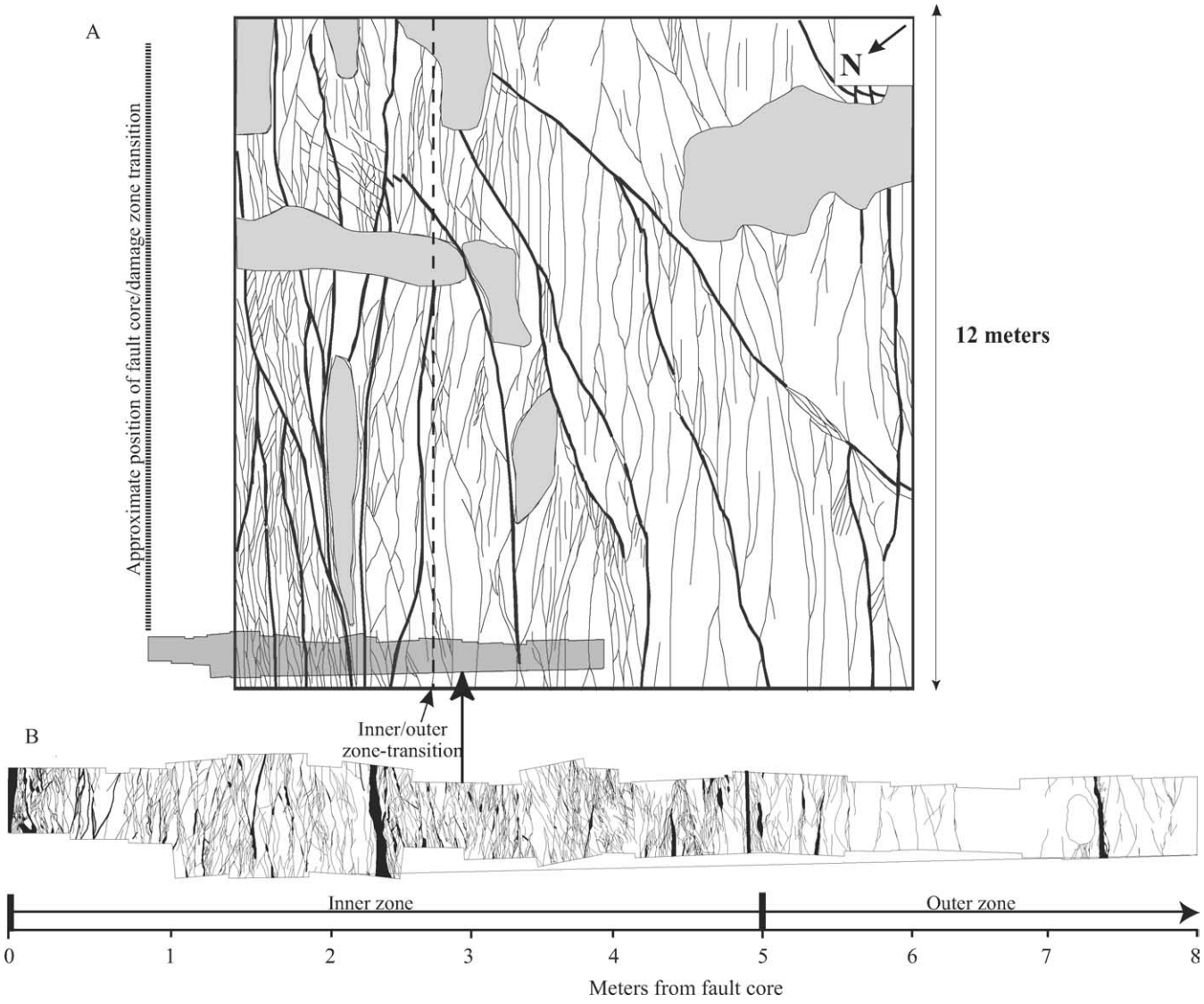

Fig. 7. Trace maps of deformation bands and zones of deformation bands of the footwall damage zone, Moab Member. (a) Distribution of deformation bands in a 12×12 m^2 area proximal to the fault core. The thick lines represent dominant zones of deformation bands. Gray-shaded areas are covered. The two maps are partly overlapping. (b) Transect showing the detailed distribution of deformation bands in an area 0–8 m from the fault core.

and 58 m, respectively. Thus, there seems to be a considerably higher concentration of strain in the thinner parts compared to the wider parts of the footwall damage zone. This relation is partly associated with the appearance of the inner zone, as the average frequency in the outer and transitional zones in the Moab Member is relatively similar (3.1–3.6 deformation bands per meter). It suggests a relatively homogenous strain distribution within each of the sub-zones, with the exception of the outer and the transitional zones in the Slick Rock Member, where the average frequency is relatively low compared with that of the Moab Member (Table 2).

4.2. Characteristics of the hanging wall damage zone

In contrast to the footwall, bedding in the hanging wall is tilted in a more than 210-m-wide, fault parallel syncline (Fig. 8a). The general trend of the affected beds is

Fig. 6. Deformation band frequency and cumulative frequency (%) vs. distance from the fault core (0 m) into the footwall. (a) Conceptual sketch showing the idealized cumulative frequency curve distinctive of three different zones based on its shape and gradient. The inner zone coincides with a linear, high gradient curve, the outer zone gives a curved to semi-linear curve, whereas a transitional zone is defined where the curve is linear with a low gradient. The frequency profiles are sampled in (b) Moab Member, Canyon B (Locality 1), (c) Moab Member, Canyon B (locality 1) 10 m SE of profile in (b), (d) Slick Rock Member, Bartlett Wash (locality 4), and (e) Moab Member, Hidden Canyon (locality 2).

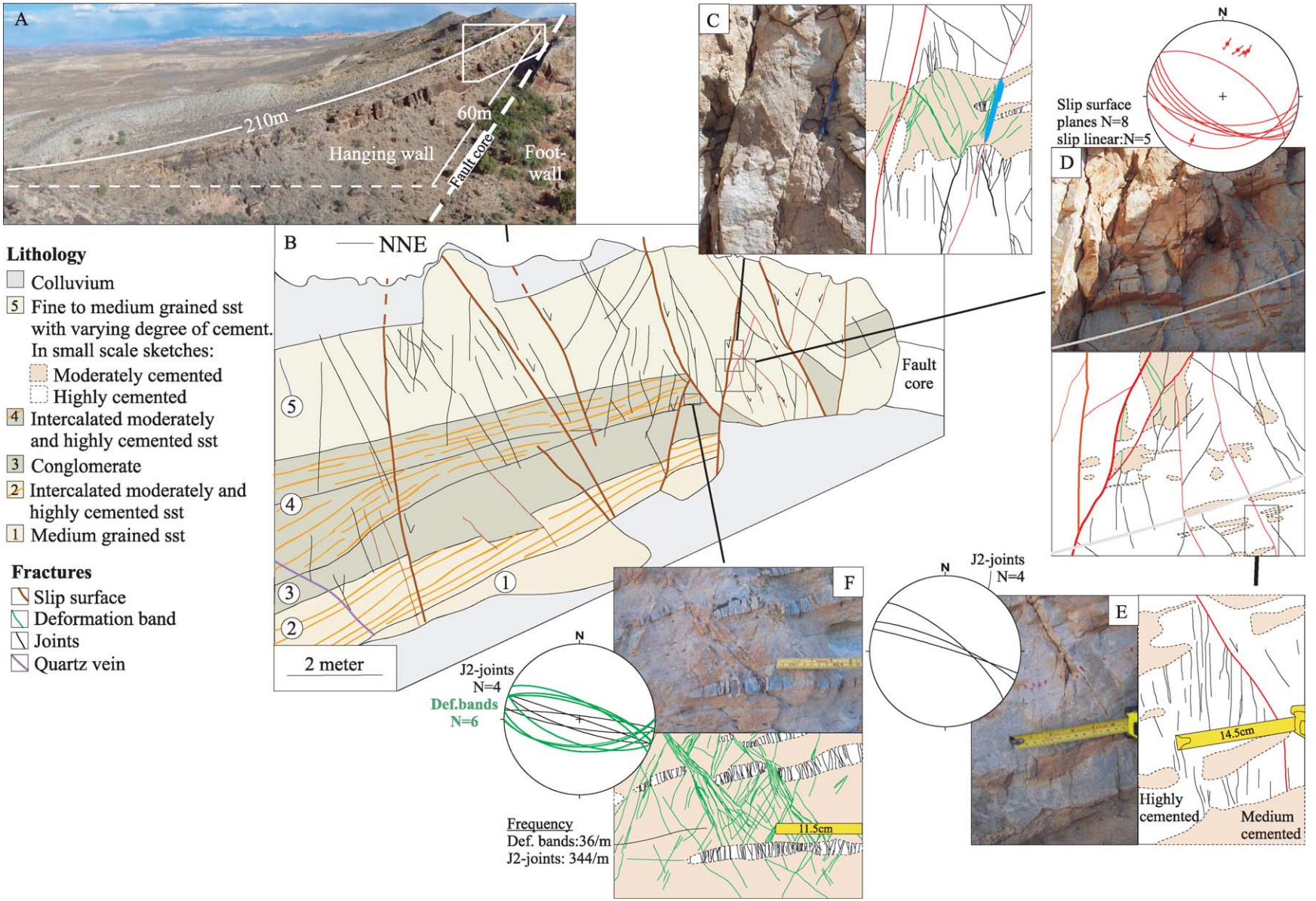

Fig. 8. (a) Photograph overview of the hanging wall syncline exposed in the southeast side of Waterfall Canyon. Displacement accommodated by the fold is indicated. (b) Simplified sketch from the innermost 14 m of the hanging wall damage zone, where the main lithological units and the largest slip surfaces and joints are indicated. (c) Close up from unit 5, illustrating the distribution of deformation bands and joints relative to the moderate and highly cemented sandstone. See pen for scale. (d) Close up from unit 5, illustrating variation of cementation patterns, and associated distribution of slip surfaces, deformation bands, and joints. See measuring tape for scale. (e) Close up from lower right part of (d). Joints are numerous within the highly cemented parts in the footwall of a minor slip surface. (f) Close up of unit 4, indicating the distribution of deformation bands and joints relative to moderate and highly cemented sandstone. The orientations of fractures are illustrated in (d)–(f). The slip linear plot incorporated in (d) show slip directions of slip surfaces measured at this locality.

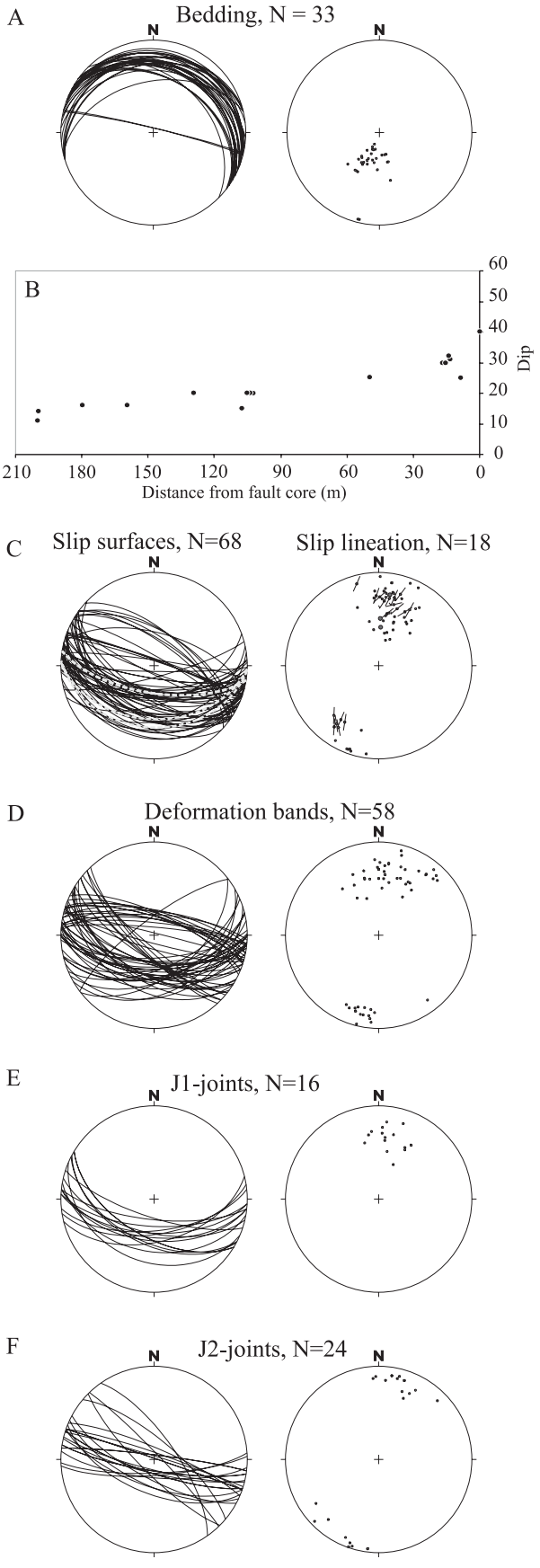

WSW–ENE to NW–SE, with a northeasterly dip (Fig. 9a). The general dip of the bedding increases gradually from sub-horizontal (ca. 10°) close to the margins of the fault zone to ca. 40° adjacent to the fault core (Fig. 9b). The syncline accommodates approximately 60 m of the total displacement of the fault zone (Fig. 8a). Observations from Mill Canyon 4–5 km ESE of the main localities show a 0.5-m-thick, highly sheared layer of shale in the hanging wall, indicating layer parallel slip. As damage zones commonly are defined by the occurrences of fractures, folds and other fault related structures (Caine et al., 1996), the damage zone width can be inferred by the syncline. From this definition, the damage zone is more than three times wider in the hanging wall compared with that in the footwall.

4.2.1. Fracture types

Slip surfaces are the most extensive and prominent fractures, and represent mainly synthetic and antithetic normal faults relative to the master fault zone (Fig. 9c). Antithetic faults predominate and account for nearly 80% of the observed slip surfaces. Reverse faults are also present, but are of minor importance. The slip surfaces are non-stratabound, and are occasionally associated with calcite and quartz mineralization. The strike of the slip surfaces ranges from WSW–ENE to NW–SE (Fig. 9c); however, most strike subparallel to the overall strike of the master fault (WNW–ESE), similar to the footwall. The synthetic slip surfaces dip 60–85° to the NNE, whereas the antithetic slip surfaces dip 23–85° to the SSW. The latter shows considerable variation in dip angle compared with the synthetic slip surfaces, as well as the slip surfaces in the footwall. There is no systematic variation in orientation of the slip surfaces vs. distance from the fault core (Fig. 10). Although the slip surfaces have a dominant dip-slip displacement, slickenlines indicate a small component of lateral slip (Fig. 9c). The observations indicate a consistent dextral component on the antithetic slip surfaces and a sinistral component on the synthetic slip surfaces.

Deformation bands are constrained to the moderately cemented sandstone (Fig. 8c, d and f). The dominant strike is SW–NE and NW–SE (Fig. 9d), being largely subparallel to the strike of the master fault. Most deformation bands are antithetic (SSW-dipping) (72%). The dips of the antithetic deformation bands in the hanging wall are also generally shallower compared with the majority of those in the footwall. The deformation bands appear throughout the exposed sections of the syncline where the moderately cemented sandstone is present; however, they are more frequent (up to 36 deformation bands per meter) in the interval between 0 and 30 m from the fault core (Fig. 11a).

Fig. 9. Orientation data from the hanging wall. (a) Bedding, (b) dip of the bedding vs. distance from fault core, (c) slip surfaces (planes marked in stippled gray are reverse slip surfaces), (d) deformation bands, (e) J1-joints, and (f) J2-joints. Equal area, lower hemisphere stereo-net, data plotted as planes, poles to planes, and slip linear.

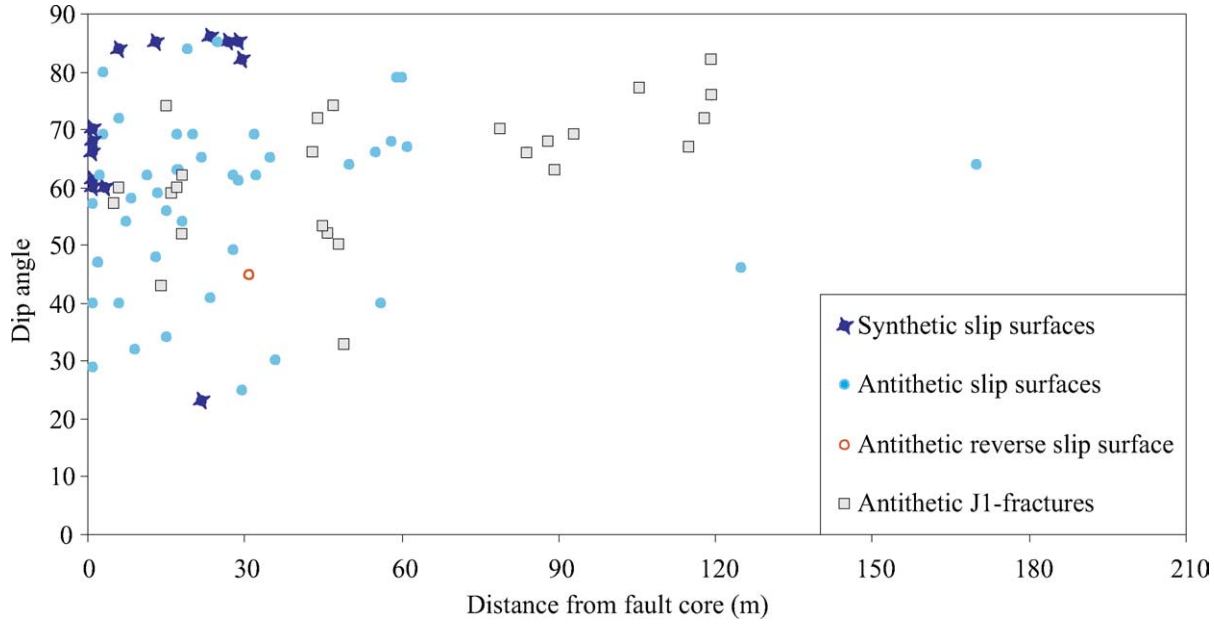

Fig. 10. Dip of slip surfaces and joints vs. distance from the fault core into the hanging wall.

Joints are sub-divided into two groups based on their spatial occurrence and length in dip direction. The *first sub-group (J1)* are non-stratabound (Fig. 8b). These joints are generally more extensive compared with the other sub-group and have lengths on the order of a few dm to several m (in dip direction). Most dip moderately to the SSW (33–74°, Fig. 9e), and are subparallel to the antithetic slip surfaces and deformation bands described above. They appear throughout all the studied outcrops of the syncline. They are, however, more frequent in the area characterized by an increase in slip surfaces (0–30 m from fault core). Similar to the slip surfaces, these fractures show no systematic variation in orientation vs. distance from the fault core (Fig. 10). Although these fractures have no visible displacement, and otherwise display the same surface morphology as the slip surfaces, this sub-group may represent slip surfaces with infinitesimal displacement. The *second sub-group (J2)* includes joints that are constrained to the highly cemented sandstone (Fig. 8c–f). These joints are generally very thin with traces shorter than 30 cm. The lengths of the traces are often constrained by the cemented beds, and are therefore stratabound (Fig. 8f). Contrary to the majority of the other fractures of the hanging wall, these fractures are sub-vertical (Fig. 9f).

4.2.2. Spatial fracture distribution

The deformation bands appear solely in the less cemented sandstone and are therefore not as widely

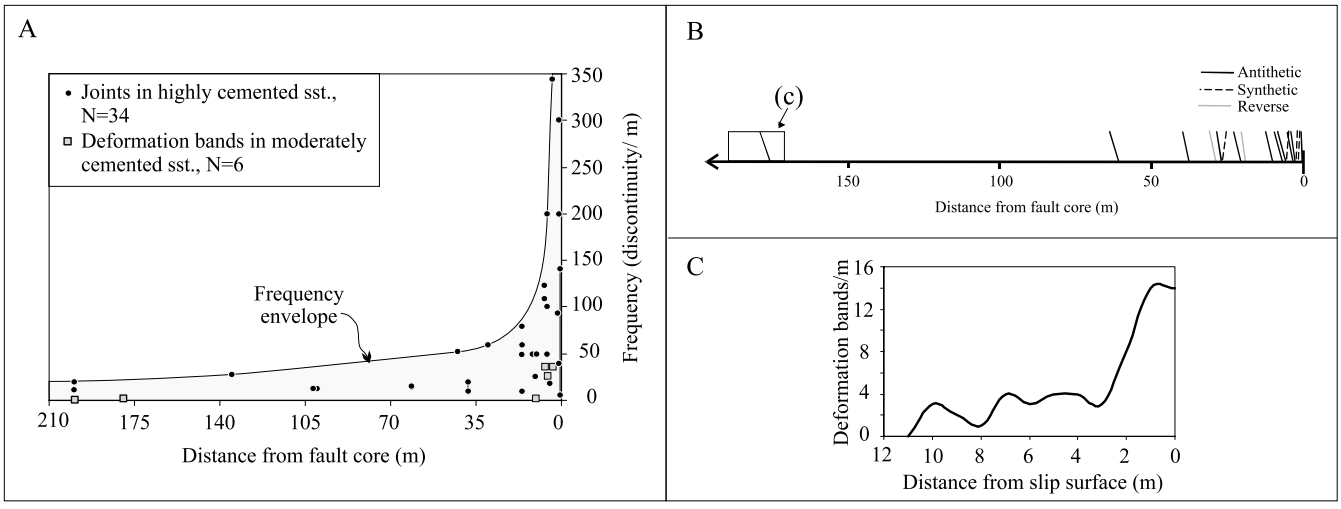

Fig. 11. (a) Fracture frequency vs. distance (m) from the fault core into the hanging wall. Based on measurements in moderately and highly cemented sandstone. (b) Distribution of dominant subsidiary fault zones with distance from the fault core (m) into the hanging wall. Location of (c) is indicated. (c) Example of the local frequency of deformation bands associated with dominant slip surface.

distributed as in the footwall damage zone. Accordingly, a sub-division into an inner and outer zone as made for the footwall is less straightforward. There is, however, a 30 m wide zone out from the fault core into the hanging wall with an increased frequency (Fig. 11a and b). In this zone the fracture frequency varies according to the lithology, and for each lithology, there seems to be a gradual decrease in fracture frequency with distance to the fault core. Therefore, the distinction between sub-zones in the hanging wall is less clear than in the footwall damage zone.

Similar to the footwall, many of the fractures and deformation bands in the hanging wall damage zone are spatially associated within subsidiary fault zones, suggesting that they are genetically related (Fig. 8c–e). Consequently, the central slip surfaces seem to contribute to the local frequency of structures (Fig. 11c). These slip surfaces are commonly several meters in length, and cut through the entire outcrop (Fig. 8b). They show the largest displacements (up to several meters). The surrounding structures represent minor synthetic and antithetic slip surfaces, antithetic J1-joints, deformation bands, and sub-vertical J2-joints, the occurrence of the latter two clearly dependent on the lithology (Fig. 8b–f).

5. Discussion

In the previous sections, we show that there are clear differences in damage zone characteristics of the footwall and hanging wall (Fig. 2). These include: (1) orientation of bedding, (2) damage zone width, (3) fracture and deformation band distribution, and (4) fracture orientation. In this section, we first discuss the results in light of general fault architecture models. Secondly, we consider relevant factors that may contribute to the asymmetric strain distribution, and evaluate possible mechanisms responsible for the observed deformation pattern.

5.1. Asymmetric strain characteristics

The above descriptions document that the footwall and the hanging wall side of the fault core display distinctively different characteristics in terms of lithology and structural arrangement. Consequently, as an extension of the general model for fault zone architecture as described by Caine et al. (1996), which distinguish between the fault core and the damage zone, we find it appropriate to divide the damage zone into two separate parts according to their location relative to the fault core: the hanging wall damage zone and the footwall damage zone.

The hanging wall part of the damage zone is more than three times wider compared with the footwall part. The hanging wall is characterized by a more than 210-m-wide syncline, and it has a larger number of antithetic fractures and deformation bands compared with the footwall part (Fig. 2). It also displays a larger spread in fracture dip angle compared with the footwall. Moreover, based on structural style and accommodated strain, we sub-divide the damage zone in the footwall into relatively homogenous sub-zones (i.e. inner, outer, and transitional zones), whereas in the hanging wall, such a sub-division is less straightforward (Fig. 2).

An asymmetric deformation pattern across normal faults is also described elsewhere in many different geological settings and on a range of scales (Aydin and Johnson, 1978; Antonellini and Aydin, 1995; Knott et al., 1996; Gabrielsen et al., 1998; Aarland and Skjerven, 1998; Hesthammer and Fossen, 1998; Nelson et al., 1999; Mitra and Ismat, 2001). For example, Koestler and Ehrman (1991) and Aarland and Skjerven (1998) reported wider hanging wall damage zones compared with the footwall damage zones of faults in the northern North Sea, whereas Doughty (2003) described the opposite case from a fault in the Rio Grande rift. In addition, faults hosted by unconsolidated sediments (Clausen et al., 2003) and the faults studied by Aarland and Skjerven (1998) show discontinuities that have more gentle dips in the footwall compared with the hanging wall. Fossen and Hesthammer (1998) described synthetic faults in both the hanging wall and footwall, where those of the hanging wall are more steeply dipping. These observations suggest that inclined faults develop asymmetric fault zone architecture as suggested by Braathen and Gabrielsen (1998), with a threefold subdivision of a fault zone into a fault core, a footwall damage zone and a hanging wall damage zone (Fig. 2).

5.2. Mechanisms controlling strain asymmetry

The asymmetric strain distribution across normal fault zones depends on several factors, such as the host rock, layer thickness, irregularities along the fault trace, displacement, and the relative position to the inclined fault core. In the following, we discuss the implications and relative importance of these factors.

5.2.1. Effect of lithology and layer thickness

In the hanging wall, the fracture distribution is clearly related to the lithology, including the distribution of cement. In the footwall, the strain intensity in the outer and transitional zones varies between the Moab and the Slick Rock Members consistent with a lithological control on the fracturing (Fig. 2). Similar results are found in poorly lithified sediments such as described by Heynekamp et al. (1999), who show that the damage zone width varies with grain size. These conclusions are supported by fracture distribution analyses that show a close relationship to lithology (Peacock and Zhang, 1993; Ouenes, 2000), layering (Peacock and Sanderson, 1992; Patton et al., 1998; Gillespie et al., 1999; Wilkins and Gross, 2002), and bedding thickness (Aarseth et al., 1997; Patton et al., 1998; Ouenes, 2000). The difference in fracturing across lithologies may reflect the different mechanical properties of the

host rock, which in turn control strengthening and weakening processes in fault zones (Heynekamp et al., 1999). It is also possible that the development of the inner zone of the footwall damage zone was controlled by lithology. Differences in mechanical properties across the fault may have had a major impact on the location of this zone, although other mechanisms, such as damage zone degradation by asperity bifurcation and segment splaying and amalgamation (Gabrielsen and Clausen, 2001), may have contributed to remove the inner zone from the hanging wall. Thus, the lithology and/or processes related to the development of the fault core may explain why an inner zone is not present in the hanging wall.

Aarland and Skjerven (1998) also have suggested that the *fracture dip angle* across faults is influenced by lithological contrasts. In the Bartlett fault, it is possible that the dip of the J2-joints is controlled by the lithology, as they only occur in the highly cemented sandstone. However, as the slip surfaces and J1-joints have consistent dip angles across lithological boundaries, factors other than lithology seem to control the dip angles of these features. We therefore expect additional factors to control the major differences in fracture orientation between the footwall and hanging wall.

We could also suspect that *damage zone width* is controlled solely by lithology. Observations from the Moab Member, which has a relatively homogenous lithology and a continuous thickness, show that there is a considerable variation in damage zone width (36–70 m) within a 300 m interval parallel to the strike of the fault. Therefore, no obvious link exists between the width of the damage zone and the host rock properties. Consequently, while the internal distribution of fractures and the dip angles of J2-joints in part is controlled by lithology and layer thickness, it is less likely that the lithological contrast alone controls the described strain differences across the fault.

5.2.2. Irregularities of the fault core and displacement

The damage zones may also be influenced by *irregularities of the fault trace* (Aarland and Skjerven, 1998; Gabrielsen et al., 1998) and *displacement*. In particular, the difference in *damage zone width* and *dip angles* may be associated with irregularities associated with the fault core. For example, linkage of two fault segments often results in a deformation halo (Peacock, 2002). Aarland and Skjerven (1998) explain the differences in dip angle across faults partly by stress perturbation associated with a ramp–flat–ramp geometry of the main fault. Furthermore, several authors have shown a positive correlation between *damage zone widths* and *displacement* (Knott, 1994; Knott et al., 1996; Beach et al., 1997, 1999; Fossen and Hesthammer, 2000; Shipton and Cowie, 2001), although these correlations all occur within strain hardening porosity lithologies (Shipton and Cowie, 2003). Based on our data, we are unable to infer the full geometry of the main fault trace and the detailed displacement profile along the fault zone. Nevertheless, the difference in width between the hanging wall and footwall cannot be explained solely by displacement, since both damage zones have suffered from the same amount of slip at a given point along the fault. Effects of irregularities of the fault core will be further discussed in association with the formation of the inner zone of the footwall damage zone in Section 5.3.

5.2.3. Position relative to the fault core: development of the syncline and the associated stress configuration

The asymmetric strain distribution may be linked to the development of the *syncline* and an *asymmetric stress distribution* associated with the fault growth. In particular, the difference in fracture dip angle, relative distribution of synthetic and antithetic faults, and difference in the damage zone width across the fault zone may be associated with the development of the syncline. The syncline has been previously described as a drag fold (Koestler et al., 1994, 1995; Foxford et al., 1996, 1998). Since the criteria for defining different types of extensional folds are somewhat unclear, we assume the drag fold terminology was used in the sense of a deflection of bedding adjacent to the fault surface (Fossen and Hesthammer, 1998), and not in the sense of the mechanism (Janecke et al., 1998; Khalil and McClay, 2002). Consequently, the syncline may represent several potential fold types associated with normal faulting (extensional folds).

Based on the stratigraphic and mechanical layering of the hanging wall, i.e. a sequence of mudrocks (Brushy Basin Member) overlain by a heterolithic section of silt- and sandstone and conglomerates (Cedar Mountain Formation), and the observations from the hanging wall in Mill Canyon (4–5 km ESE) where a layer of shale shows layer parallel slip, it is possible that folding is accommodated largely by flexural slip. Three possible scenarios of folding, partly accommodated with flexural slip, are considered (Fig. 12). They involve development of (1) a drag fold, (2) an antilistric fault bend fold, and (3) a fault propagation fold.

The *drag fold* scenario relates to frictional resistance along the fault core (Fig. 12a) (Janecke et al., 1998; Khalil and McClay, 2002). This mechanism should in principle affect both the footwall and the hanging wall. In addition, intense fracturing in the vicinity of the fault core should be expected. Apart from a relatively high density of fractures and deformation bands near the fault core, there are no clear indications of a drag fold. The same applies to the internal deformation of *antilistric fault bend folds*, which is the second scenario (Fig. 12b). Studies dealing with hanging wall deformation associated with antilistric fault bend fold focus on the overall structural geometries rather than the detailed internal geometry of the fold (Ferrill and Morris, 1997; Ferrill et al., 2005). Moreover, we are unable to infer the original geometry of the fault trace above and below the exposed section. Consequently, we cannot relate our observations from the hanging wall syncline of the Bartlett fault directly to the characteristics of an antilistric fault bend fold or a drag fold.

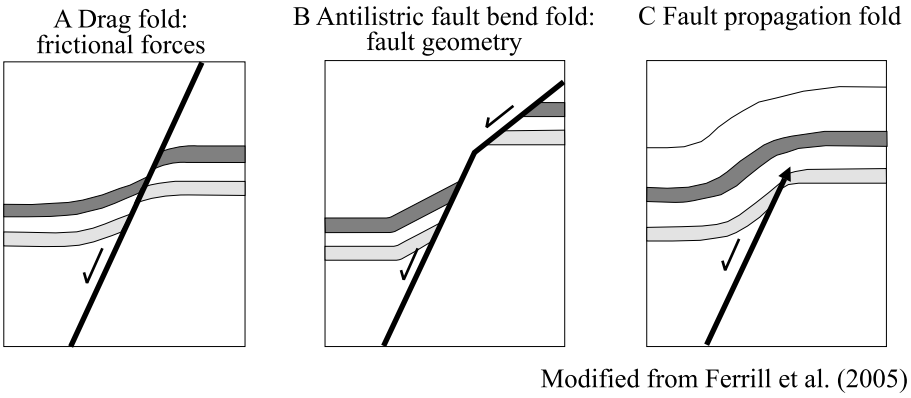

Fig. 12. Scenarios for syncline development.

There has been a recent focus on subsidiary structures associated with *fault propagation folds* (Fig. 12c), both from field exposure (Gawthorpe et al., 1997), sub-surface data (Fossen and Hesthammer, 1998), and analog experiments (Withjack et al., 1990; Withjack and Callaway, 2000). Analog experiments involving forced folds (Withjack et al., 1990; Withjack and Callaway, 2000) show a distribution of synthetic and antithetic fractures across the fault zone (Fig. 13a) that is strikingly similar to the distribution observed across the Bartlett fault. More specifically, in the analog experiments, there is a predominance of synthetic faults in the footwall and antithetic faults in the hanging wall, similar to the larger subsidiary fault zones and slip surfaces of the Bartlett fault. In addition, both in the experiments by Withjack et al. (1990) and Withjack and Callaway (2000), and field examples of fault propagation folds (Gawthorpe et al., 1997), a small number of reverse faults are observed. These may represent analogs to the reverse faults present in the hanging wall of the Bartlett fault. These similarities suggest that many of the damage zone structures (especially in the hanging wall) were formed during development of a fault propagation fold, as illustrated in Fig. 13b. The fault propagation fold model is further supported by interpretations by Ferrill et al. (2005), who apply the hanging wall syncline as an example for synthetic dip caused by fault propagation folding (faulted tip-line folding). Fold-induced fracturing in the hanging wall can also be inferred from the variation in fracture dip angle. Many of the antithetic structures in the hanging wall, apart from the J2-joints, have a lower dip angle compared with that of the footwall and, in general, there is a widespread distribution in dip for up to several tens of meters into the hanging wall (e.g. Fig. 10). This suggests a possible relation between the development of the syncline and the formation and subsequent rotation ($\sim$40° at the most) of discontinuities.

Fold-induced fracturing of the hanging wall may therefore be related to the dynamic, inhomogeneous stress field associated with the formation of the syncline. Lewis et al. (2002) report significant stress perturbations of fault-related folding, especially on the downthrown side of the fault, resulting in strong asymmetry in stress about the fault. By using this analog, we infer that the damage zone fractures and deformation bands developed in an asymmetric stress field, and that differences related to (1) the width of the footwall and hanging wall damage zones and (2) the

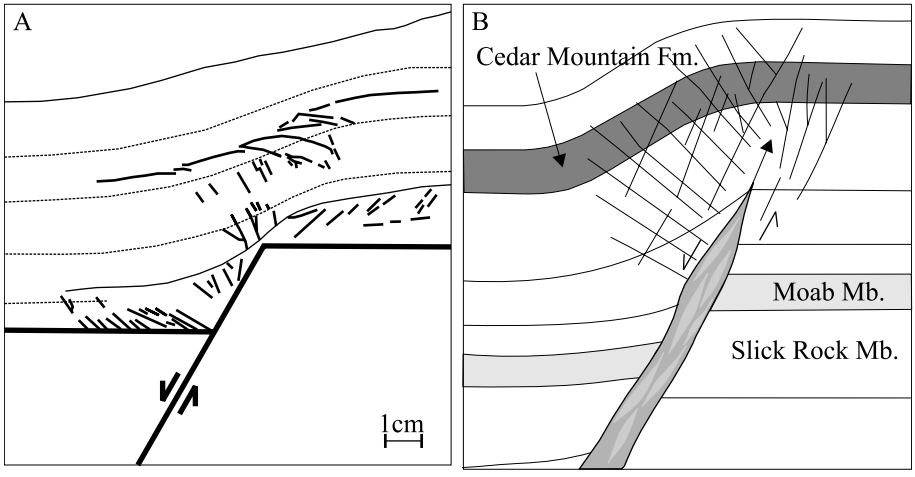

Fig. 13. (a) Cross-section from multilayer experiment with 60° dipping normal fault. It shows the development of a forced fold (fault propagation fold) and secondary faults. Modified from Withjack et al. (1990). (b) Illustration of fault-related fractures and their relation to development of the syncline.

orientation of deformation bands and slip surfaces across the fault are controlled by the stress distribution associated with the progressive development of a fault propagation fold.

5.3. Formation of the inner zone

The inner zone of the footwall damage zone represents characteristics that are different from other parts of the damage zones. As discussed above, the reason why the inner zone is not found in the hanging wall may be related to the lithology or to processes causing damage zone degradation (Gabrielsen and Clausen, 2001). However, these factors cannot explain the difference in strain intensity between the inner and outer zones of the footwall damage zone, where the lithology is relatively homogenous. A key issue is which mechanisms control this difference. We consider four possible mechanisms that may have contributed. These include: (1) strain associated with a propagating fault tip (process zone model), (2) widening a fault zone due to strain hardening and softening (modified slip-patch model) (Shipton and Cowie, 2003), (3) fracturing caused by seismic waves ('dynamic stresses') (Kilb et al., 2000; Gomberg et al., 2001; Vidale and Li, 2003), and (4) combined local restraining and releasing bends associated with irregularities along the fault core boundaries.

A *fault process zone* is commonly described as a zone of microscopic fractures developing ahead of a propagating fault tip (Anders and Wiltschko, 1994; Vermilye and Scholz, 1998). Process zones with macroscopic deformation bands have also been described (Shipton and Cowie, 2001, 2003). In particular, Shipton and Cowie (2001) infer that process zones associated with continuous slip surfaces in porous sandstone consist of clusters of deformation bands and isolated slip surfaces. These zones are expected to be 5–12 m wide and a few hundred meters long, consistent with the dimensions of the inner zone in the Bartlett fault. According to the slip-patch model described by Shipton and Cowie (2003), such zones develop through accumulation of strain through several ruptures, each forming individual process zones within a limited range around the fault core. We expect the Bartlett fault to have a history with several slip events, which is likely based on the scale of displacement. Also, since the characteristics of the inner zone is compatible with the zones described by Shipton and Cowie (2001), the process zone model cannot be ruled out.

In the *modified slip-patch model*, Shipton and Cowie (2003) expand these principles by including the effects of strain hardening and strain softening to explain widening of the damage zones with increasing displacement. The damage zones expand as a result of slip along structures in the damage zone, each forming their own, local process zone. This would form a hierarchy of subsidiary fault zones, as is observed in the hanging wall damage zone and in the outer and transitional zones of the footwall damage zone of the Bartlett fault. The model also predicts that process zones occur along the margins of these subsidiary faults. Although there are local clusters of deformation bands, the deformation pattern associated with subsidiary faults outside the inner zone are fundamentally different from that in the inner zone. This is evident from both the fracture frequency and the interaction of the deformation bands summarized in Fig. 2. We therefore suggest that the deformation mechanisms controlling the development of the inner zone were different from those affecting the outer and transitional zones. Thus, the modified slip-patch model is not suitable to explain the development of the inner zone.

It has also been suggested that strong *seismic waves* can cause fault damage (Kilb et al., 2000; Gomberg et al., 2001; Vidale and Li, 2003). Specifically, it is inferred that transient, oscillatory stress changes transmitted as seismic waves (i.e. dynamic stresses) can trigger earthquakes, both as a direct response (increased fluid pressure) and due to a cyclic reduction in the strength of the rock (fatigue) (Gomberg et al., 2001). Gomberg et al. (2001) reported that both static stress changes and dynamic stresses seem important for triggering in the near field of a hypocenter, suggesting that some of the deformation in the damage zones could relate to seismic waves. In the case of the Bartlett fault, it is difficult to delineate fractures that were influenced by dynamic stresses, since prediction of movement and magnitude of seismic waves associated with fault growth requires further analyses. There are, however, reasons to expect the effect of dynamic stresses is stronger in the direction of fault tip propagation. Seismic waves are more likely to interact and amplify in the vicinity of their source (Stein and Wysession, 2003) since new waves continuously radiate during rupture. Thus, the likelihood for wave interaction is greatest in the propagation direction. This reasoning is further supported by laboratory experiments by Xia et al. (2004), who visualize shear waves ahead of a rupturing front. The effect of the interacting waves may be a reduction of the local fluid pressure and subsequent failure. Based on these principles, we suggest that seismic waves can contribute in deformation associated with development of the process zone. Consequently, if the process zone model applies to the development of inner zone, we suspect that seismic waves were involved in the development of the inner zone.

An alternative hypothesis for the inner zone relates to *local restraining and releasing bends* associated with irregularities along the fault core boundaries (Fig. 14). The fault core consists of a variety of lithologies, including elongate bodies of host rock (horses), as is described from faults in several geological settings (Childs et al., 1996; Clausen et al., 2003; Doughty, 2003; Lindanger, 2003). Incorporation of horses into the fault core involves a number of mechanisms, including segment linkage, tip-line bifurcation, asperity bifurcation, and segment splaying/amalgamation (Childs et al., 1996; Gabrielsen and Clausen, 2001). Most of these configurations result in irregular geometries along the margins of the core, as is observed along the fault core of the Bartlett fault (e.g. 3a and b).

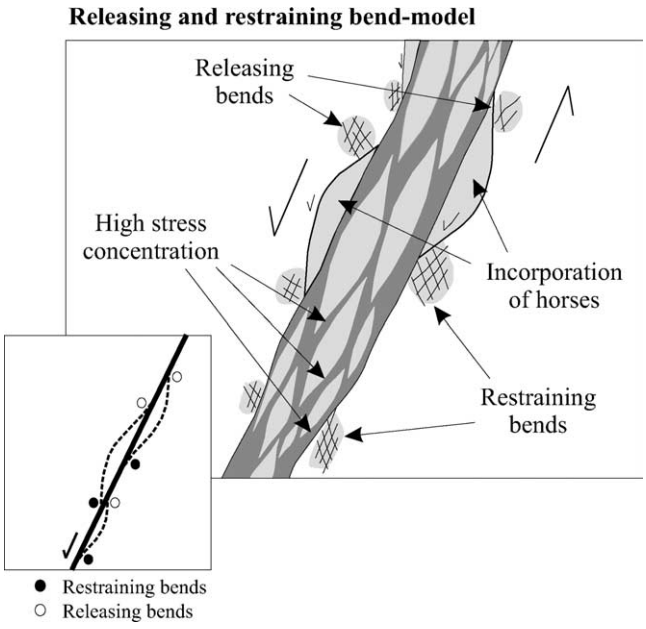

Fig. 14. Conceptual model for the development and high frequency of deformation bands adjacent to the fault core (inner zone).

During faulting, such irregular margins may represent local restraining and releasing bends that cause significant stress build-ups or disturbances at localized sites (Fig. 14). These sites may cause major damage to the adjacent rock. The development of the fault core and its surroundings cause local changes in the stress field, and thereby progressively affect various parts along the strike and dip of the fault core. In this way, a considerable portion of the near field of the fault core is affected over time. Thus, zones with increased distance from the core (i.e. outer and transitional zones) will not be affected to the same degree. This hypothesis may also explain why the inner zone at some places is absent, since processes involved during growth of the fault core also lead to degradation of the damage zone (Gabrielsen and Clausen, 2001). We therefore favor the combined restraining and releasing bend hypothesis in explaining the formation of the inner zone.

6. Conclusions

Outcrop data obtained along the Bartlett segment of the Moab Fault, SE Utah, demonstrate that the characteristics of the damage zones across the fault zone are strongly asymmetric. The main differences between the footwall and hanging wall damage zones are related to: (i) the folded bedding of the hanging wall with a gradual increase in dip towards the fault core (maximum of 40°) in contrast to the sub-horizontal orientation of bedding in the footwall. (ii) The damage zone of the hanging wall is three times wider than the footwall damage zone. (iii) The fracture and deformation band distributions differ between the two damage zones in that the inner ($\leq$5 m wide) zone of the footwall has a relatively high frequency of deformation bands (up to 55 fractures/m) compared with the other parts of the damage zones. In addition, the fracture and deformation band distribution in the hanging wall is more complex. (iv) Antithetic structures are more abundant in the hanging wall (70–80%) compared with the footwall (55%). (v) The antithetic structures in the hanging wall are generally more gently dipping than those of the footwall. Based on these differences, we find it appropriate to divide the damage zone of the Bartlett fault into two separate parts according to their location relative to the inclined fault zone: *the footwall damage zone* and *the hanging wall damage zone*.

The observed deformation pattern is influenced by the lithology and/or by processes associated with the development of the fault core (releasing/restraining bends, asperity bifurcation, and segment linkage). The most important cause of the asymmetric deformation pattern is, however, related to the asymmetric stress field that develops during fault propagation and folding of the hanging wall.

Acknowledgements

We thank Alvar Braathen and Roy H. Gabrielsen for motivating discussions and comments on the early versions of this manuscript. We are also grateful to Zoe Shipton, Nick Davatzes and David A. Ferrill for constructive reviews, Kuvvet Atakan and Haakon Fossen for fruitful discussions, and Tord E.S. Johansen and Richard Kluge for an enjoyable time in the field. The Research Council of Norway provided financial support for this research.

References

Aarland, R.K., Skjerven, J., 1998. Fault and fracture characteristics of major fault zone in the northern North Sea: analyses of 3D seismic and oriented cores in the Brage Field (Block 31/4). In: Coward, M.P., Daltaban, T.S., Johnson, H. (Eds.), Structural Geology in Reservoir Characterization, vol. 127, pp. 209–229.

Aarseth, E.S., Bourgine, B., Castaing, C., Chilès, J.P., Christenson, N.P., Eeles, M., Fillion, E., Genter, A., Gillespie, P.A., Håkansson, E., Zinck Jørgensen, K., Lindgaard, H.F., Madsen, L., Odling, N.E., Olsen, C., Reffstrup, J., Trice, R., Walsh, J.J., Watterson, J., 1997. Interim guide to fracture interpretation and flow modelling in fractured reservoirs. European Commission, Brussels, 203.

Anders, M.H., Wiltschko, D.V., 1994. Microfracturing, paleostress and the growth of faults. Journal of Structural Geology 16 (6), 795–815.

Antonellini, M., Aydin, A., 1994. Effect of faulting on fluid flow on porous sandstones: petrophysical properties. American Association of Petroleum Geologists Bulletin 78 (3), 355–377.

Antonellini, M., Aydin, A., 1995. Effect of faulting on fluid flow on porous sandstones: geometry and spatial distribution. American Association of Petroleum Geologists Bulletin 79 (5), 642–671.

Aydin, A., 1978. Small faults formed as deformation bands in sandstone. Pure and Applied Geophysics 116, 913–930.

Aydin, A., Johnson, A.M., 1978. Development of faults as zones of deformation bands and slip surfaces in sandstone. Pure and Applied Geophysics 116, 931–942.

Beach, A., Brown, J.L., Welbon, A.I., McCallum, J.E., Brockbank, P., Knott, S., 1997. Characteristics of fault zones in sandstone from NW England: application to fault transmissibility. In: Meadows, N.S., Trueblood, S.P., Hardman, M., Cown, G. (Eds.), Petroleum Geology of the Irish Sea and Adjacent Areas Geological Society Special Publication No. 124, pp. 315–324.

Beach, A., Welbon, A.I., Brockbank, P.J., McCallum, J.E., 1999. Reservoir damage around faults: outcrop examples from the Suez rift. Petroleum Geoscience 5 (2), 109–116.

Braathen, A., Gabrielsen, R.H., 1998. Lineament architecture and fracture distribution in metamorfic and sedimentary rocks, with application to Norway. Geological Survey of Norway, Trondheim, 78.

Bruhn, R.L., Parry, W.T., Yonkee, W.A., Thompson, T., 1994. Fracturing and hydrothermal alteration in normal fault zones. Pure and Applied Geophysics 142 (3/4), 609–644.

Caine, J.S., Evans, J.P., Forster, C.B., 1996. Fault zone architecture and permeability structure. Geology 24 (11), 1025–1028.

Chester, F.M., Logan, J.M., 1986. Implications for mechanical properties of brittle faults from observations of the Punchbowl fault zone, California. Pure and Applied Geophysics 124 (1/2), 79–106.

Chester, F.M., Logan, J.M., 1987. Composite planar fabric from Punchbowl Fault, California. Journal of Structural Geology 9 (5/6), 621–634.

Chester, F.M., Evans, J.P., Biegel, R.L., 1993. Internal structure and weakening mechanisms of the San Andreas Fault. Journal of Geophysical Research 98 (B1), 771–786.

Childs, C., Watterson, J., Walsh, J.J., 1996. A model for the structure and development of fault zones. Journal of Geological Society, London 153, 337–340.

Clausen, J.A., 2002. The sealing capacity and architecture of shallow faults in sedimentary sequences. Unpublished Dr Scient. Thesis, University of Bergen.

Clausen, J.A., Gabrielsen, R.H., Johnsen, E., Korstgård, J.A., 2003. Fault architecture and clay smear distribution. Examples from field studies and drained ring-shear experiments. Norwegian Journal of Geology 83 (2), 131–146.

Davatzes, N.C., Aydin, A., 2003. Overprinting faulting mechanisms in high porosity sandstones of SE Utah. Journal of Structural Geology 25 (11), 1795–1813.

Doelling, H.H., 2001. Geologic map of the Moab and eastern part of the San Rafael Desert 30′×60′ quadrangles, Grand and Emery Counties, Utah, and Mesa County, Colorado. Utah Geological Survey.

Doughty, P.T., 2003. Clay smear seals and fault sealing potential of an exhumed growth fault, Rio Grande Rift, New Mexico. American Association of Petroleum Geologists Bulletin 87 (3), 427–444.

Evans, J.P., Forster, C.B., Goddard, J.V., 1997. Permeability of fault-related rocks, and implications for hydraulic structure of fault zones. Journal of Structural Geology 19 (11), 1393–1404.

Ferrill, D.A., Morris, A.P., 1997. Geometric considerations of deformation above curved normal faults and salt evacuation surfaces. The Leading Edge 16 (8), 1129–1133.

Ferrill, D.A., Morris, A.P., Sims, D.W., Waiting, D.J., Hasegawa, S., 2005 Development of synthetic layer dip adjacent to normal faults. In: Sorkhabi, R., Tsuji, Y. (Eds.), Faults, Fluid Flow, and Petroleum Traps, AAPG Memoir, 85, 125–138.

Forster, C.B., Evans, J.P., 1991. Hydrogeology of thrust faults and crystalline thrust sheets: results of combined field and modelling studies. Geophysical Research Letters 18 (5), 979–982.

Fossen, H., Hesthammer, J., 1998. Structural geology of the Gullfaks Field, northern North Sea. In: Coward, M.P., Daltaban, T.S., Johnson, H. (Eds.), Structural Geology in Reservoir Characterization Geological Society, London, Special Publication 127, pp. 231–261.

Fossen, H., Hesthammer, J., 2000. Possible absence of small faults in the Gullfaks Field, northern North Sea: implications for downscaling of faults in some porous sandstones. Journal of Structural Geology 22 (7), 851–863.

Foxford, K.A., Garden, I.R., Guscott, S.C., Burley, S.D., Lewis, J.J., Walsh, J.J., Watterson, J., 1996. The field geology of the Moab Fault. In: Huffman Jr.., A.C., Lund, W.R., Godwin, L.H. (Eds.), Geology and Resources of the Paradox Basin Utah Geological Association Guidebook 25, pp. 265–283.

Foxford, K.A., Walsh, J.J., Watterson, J., Garden, I.R., Guscott, S.C., Burley, S.D., 1998. Structure and content of the Moab Fault Zone, Utah, USA, and its implications for fault seal prediction. In: Jones, G., Fisher, Q.J., Knipe, R.J. (Eds.), Faulting, Fault Sealing, and Fluid Flow in Hydrocarbon Reservoirs Geological Society, London, Special Publications 147, pp. 87–103.

Gabrielsen, R.H., Aarland, R.-K., 1990. Characteristics of pre- and syn-consolidation structures and tectonic joints and microfaults in fine to medium-grained sandstone. In: Stephansson, B. (Ed.), Rock Joints. Balkema, Rotterdam, pp. 45–50.

Gabrielsen, R.H., Clausen, J.A., 2001. Horses and duplexes in extensional regimes: a scale-modeling contribution. In: Koyi, H.A., Mancktelow, N.S. (Eds.), Tectonic Modelling: A Volume in Honor of Hans Ramberg Geological Society of America Memoir 193. Geological Society of America, Boulder, CO, pp. 207–220.

Gabrielsen, R.H., Aarland, R.-K., Alsaker, E., 1998. Identification and spatial distribution of fractures in porous, siliclastic sediments. In: Coward, M.P., Daltaban, T.S., Johnson, H. (Eds.), Structural Geology in Reservoir Characterization Geological Society, London, Special Publications, pp. 49–64.

Garden, I.R., Guscott, S.C., Burley, S.D., Foxford, K.A., Walsh, J.J., Marshall, J., 2001. An exhumed palaeo-hydrocarbon migration fairway in a faulted carrier system, Entrada Sandstone of SE Utah, USA. Geofluids 1 (3), 195–213.

Gawthorpe, R., Sharp, I., Underhill, J.R., Gupta, S., 1997. Linked sequence stratigraphic and structural evolution of propagating normal faults. Geology 25 (9), 795–798.

Gibson, R.G., 1998. Physical character and fluid-flow properties of sandstone-derived fault zones. In: Coward, M.P., Daltaban, T.S., Johnson, H. (Eds.), Structural Geology in Reservoir Characteriztaion Geological Society, London, Special Publications No. 127, pp. 83–97.

Gillespie, P.A., Johnston, J.D., Loriga, M.A., McCaffrey, K.J.M., Walsh, J. J., Watterson, J., 1999. Influence of layering on vein systematics in line samples. In: McAffree, K.J.W., Lonergan, L., Wilkinson, J.J. (Eds.), Fractures, Fluid Flow and Mineralization Geological Society, London, Special Publications 155, pp. 35–56.

Gomberg, J., Reasenberg, P.A., Bodin, P., Harris, R.A., 2001. Earthquake triggering by seismic waves following the Landers and Hector Mine earthquakes. Nature 411, 462–466.

Harris, S.D., McAllister, E., Knipe, R.J., Odling, N.E., 2003. Predicting the three-dimensional population characteristics of fault zones: a study using stochastic models. Journal of Structural Geology 25 (8), 1281–1299.

Heermance, R., Shipton, Z.K., Evans, J.P., 2003. Fault structure control on fault slip and ground motion during the 1999 rupture of the Chelungpu Fault, Taiwan. Bulletin of the Seismological Society of America 93 (3), 1034–1050.

Hesthammer, J., Fossen, H., 1998. The use of dipmeter data to constrain the structural geology of the Gullfaks Field, northern North Sea. Marine and Petroleum Geology 15, 549–573.

Hesthammer, J., Johansen, T.E.S., Watts, L., 2000. Spatial relationships within fault damage zones in sandstone. Marine and Petroleum Geology 17 (8), 873–893.

Heynekamp, M.R., Goodwin, L.B., Mozley, P.S., Haneberg, W.C., 1999. Controls on fault-zone architecture in poorly lithified sediments, Rio Grande Rift, New Mexico: implications for fault-zone permeability and fluid flow. In: Goodwin, L.B., Mozley, P.S., Moore, J.M., Haneberg, W.

C. (Eds.), Faults and Subsurface Fluid Flow in the Shallow Crust Geophysical Monograph 113. American Geophysical Union, Washington, pp. 27–49.

Janecke, S.U., Vandenburg, C.J., Blankenau, J.J., 1998. Geometry, mechanisms and significance of extensional folds from examples in the Rocky Mountain Basin and Range province, USA. Journal of Structural Geology 20 (7), 841–856.

Jones, M.A., Knipe, R.J., 1996. Seismic attribute maps; application to structural interpretation and fault seal analysis in the North Sea Basin. First Break 14 (12), 449–461.

Jourde, H., Flodin, E.A., Aydin, A., Durlofski, L.J., Wen, X.-H., 2002. Computing permeability of fault zones in eolian sandstone from outcrop measurements. American Association of Petroleum Geologists Bulletin 86 (7), 1187–1200.

Khalil, S.M., McClay, K.R., 2002. Extensional fault-related folding, northwestern Red Sea, Egypt. Journal of Structural Geology 24 (4), 743–762.

Kilb, D., Gomberg, J., Bodin, P., 2000. Triggering of earthquake aftershocks by dynamic stresses. Nature 408, 570–574.

Kim, Y.-S., Peacock, D.C.P., Sanderson, D.J., 2004. Fault damage zones. Journal of Structural Geology 26 (3), 503–517.

Knott, S.D., 1994. Fault zone thickness versus displacement in the Permo-Triassic sandsones of NW England. Journal of the Geological Society, London 151, 17–25.

Knott, S.D., Beach, A., Brockbank, P.J., Brown, J.L., McCallum, J.E., Welbon, A.I., 1996. Spatial and mechanical controls on normal fault populations. Journal of Structural Geology 18 (2-3), 359–372.

Koestler, A.G., Ehrmann, W.U., 1991. Description of brittle extensional features in chalk on the crest of a salt ridge (NW Germany). In: Roberts, A.M., Yielding, G., Freeman, B. (Eds.), The Geometry of Normal Faults Geological Society, London, Special Publications 56, pp. 113–123.

Koestler, A.G., Milnes, A.G., Olsen, T.S., Buller, A.T., 1994. A structural simulation tool for faulted sandstone reservoirs: exploratory study using data from Utah and the Gullfaks field. In: Aasen, J.O., Berg, E., Buller, A.T., Hjelmeland, O., Holt, R.M., Kleppe, J., Torsæter, O. (Eds.), North Sea Oil and Gas Reservoirs-III. Kluwer Academic Publishers, Trondheim, pp. 157–165.

Koestler, A.G., Milnes, A.G., Keller, P., 1995. Quantification of fault/fracture systems for reservoir simulation—use of systematic data from field analogues. In: Olsen, J., Hinderaker, L. (Eds.), PROFIT 1990–1994. Project Summary Reports: Reservoir Characterization, Near Well Flow. Norwegian Petroleum Directorate, Stavanger, pp. 23–41.

Lewis, A.C., Olden, P., Couples, G.D., 2002. Geomechanical simulations of top seal integrity. In: Koestler, A.G., Hunsdale, R. (Eds.), Hydrocarbon Seal Quantification NPF Special Publication 11. Norwegian Petroleum Society, Amsterdam, pp. 75–87.

Lindanger, M., 2003. A study of rock lenses in extensional faults, focusing on controlling shapes and dimensions. Unpublished Cand. Scient. Thesis, University of Bergen.

Mandl, G., 1988. Mechanics of Tectonic Faulting. Models and Basic Consepts. Elsevier, Amsterdam.

Mandl, G., 2000. Faulting in Brittle Rocks. An Introduction to the Mechanics of Tectonic Faults. Springer, Berlin.

McCaig, A.M., 1988. Deep fluid circulation in fault zones. Geology 16 (10), 867–870.

Micarelli, L., Moretti, I., Daniel, J.M., 2003. Structural properties of rift-related normal faults: the case study of the Gulf of Corinth, Greece. Journal of Geodynamics 36 (1–2), 275–303.

Mitra, G., Ismat, Z., 2001. Microfracturing associated with reactivated fault zones and shear zones: what can it tell us about deformation history? In: Holdsworth, R.E., Strachan, R.A., Magloughlin, J.F., Knipe, R.J. (Eds.), The Nature and Tectonic Significance of Fault Zone Weakening Geological Society, London, Special Publications 186, pp. 113–140.

Nelson, E.P., Kullman, A.J., Gardner, M.H., 1999. Fault-fracture networks and related fluid flow and sealing, Brushy Canyon Formation, West Texas. In: Goodwin, L.B., Mozley, P.S., Moore, J.M., Haneberg, W.C. (Eds.), Faults and Subsurface Fluid Flow in the Shallow Crust Geophysical Monograph 113. American Geophysical Union, Washington, pp. 69–81.

Olig, S.S., Fenton, C.H., McCleary, J., Wong, I.G., 1996. The earthquake potential of the Moab Fault and its relation to salt tectonics in the Paradox Basin, Utah. In: Huffman Jr., A.C., Lund, W.R., Godwin, L.H. (Eds.), Geology and Resources of the Paradox Basin Utah Geological Association Guidebook 25, pp. 246–251.

Ouenes, A., 2000. Practical application of fuzzy logic and neural networks to fractured reservoir characterization. Computers and Geosciences 26 (8), 953–962.

Patton, T.L., Logan, J.M., Friedman, M., 1998. Experimentally generated normal faults in single-layer and multilayer limestone specimens at confining pressure. Tectonophysics 295 (1-2), 53–77.

Peacock, D.C.P., 2002. Propagation, interaction and linkage in normal fault systems. Earth-Science Reviews 58 (1-2), 121–142.

Peacock, D.C.P., Sanderson, D.J., 1992. Effects of layering and anisotropy on fault geometry. Journal of the Geological Society, London 149, 793–802.

Peacock, D.C.P., Zhang, X., 1993. Field examples and numerical modelling of oversteps and bends along normal faults in cross-section. Tectonophysics 234, 147–167.

Peacock, D.C.P., Knipe, R.J., Sanderson, D.J., 2000. Glossary of normal faults. Journal of Structural Geology 22, 291–305.

Pittman, E.D., 1981. Effects of fault-related granulation on porosity and permeability of quartz sandstones, Simpson group (Ordovician), Oklahoma. American Association of Petroleum Geologists, Bulletin 65 (11), 2381–2387.

Pollard, D.D., Aydin, A., 1988. Progress in understanding jointing over the past century. Geological Society of America Bulletin 100, 1181–1204.

Rawling, G.C., Goodwin, L.B., Wilson, J.L., 2001. Internal architecture, permeability structure, and hydrologic significance of contrasting fault-zone types. Geology 29 (1), 43–46.

Schulz, S.E., Evans, J.P., 1998. Spatial variability in microscopic deformation and composition of the Punchbowl fault, southern California: implications for mechanisms, fluid–rock interaction, and fault morphology. Tectonophysics 295 (1-2), 223–244.

Schulz, S.E., Evans, J.P., 2000. Mesoscopic structure of the Punchbowl Fault, Southern California and the geologic and geophysical structure of active strike-slip faults. Journal of Structural Geology 22 (7), 913–930.

Seront, B., Wong, T.-F., Caine, J.S., Forster, C.B., Bruhn, R.L., Fredrich, J. T., 1998. Laboratory characterization of hydromechanical properties of a seismogenic normal fault system. Journal of Structural Geology 20 (7), 865–881.

Shipton, Z.K., Cowie, P.A., 2001. Damage zone and slip-surface evolution over μm to km scales in high-porosity Navajo sandstone, Utah. Journal of Structural Geology 23 (12), 1825–1844.

Shipton, Z.K., Cowie, P.A., 2003. A conceptual model for the origin of fault damage zone structures in high-porosity sandstone. Journal of Structural Geology 25 (3), 333–344.

Shipton, Z.K., Evans, J.P., Robeson, K.R., Forster, C.B., Snelgrove, S., 2002. Structural heterogeneity and permeability in eolian sandstone: implications for subsurface modeling of faults. American Association of Petroleum Geologists Bulletin 86 (5), 863–883.

Sibson, R.H., 1992. Implications of fault-valve behaviour for rupture nucleation and recurrence. Tectonophysics 211, 283–293.

Sibson, R.H, 1994. Crustal stress, faulting and fluid flow. In: Parnell, L. (Ed.), Geofluids: Origin Migration and Evolution of Fluids in Sedimentary Basin Geological Society Special Publication 78, pp. 69–84.

Sibson, R.H., 1996. Structural permeability of fluid-driven fault-fracture meshes. Journal of Structural Geology 18 (8), 1031–1042.

Sibson, R.H., Scott, J., 1998. Stress/fault controls on the containment and release of overpressured fluids: examples from gold-quartz vein systems in Juneau, Alaska; Victoria, Australia and Otago, New Zealand. Ore Geology Reviews 13 (1-5), 293–306.

Smith, L., Forster, C., Evans, J., 1990. Interaction of fault zones, fluid flow, and heat transfer at the basin scale. In: Newman, S.P., Neretnieks, I. (Eds.), Hydrogeology of Low Permeability Environments Selected Papers in Hydrogeology 2. International Association for Hydrogeologists, pp. 41–67.

Stein, S., Wysession, M., 2003. An introduction to Seismology, Earthquakes, and Earth Structure. Blackwell Publishing, Cornwall.

United States Geological Survey, 1985. Merrimac Butte Quadrangle. US Geological Survey, Denver.

United States Geological Survey, 1988. Jug Rock Quadrangle. US Geological Survey, Denver.

Vermilye, J.M., Scholz, C.H., 1998. The process zone: a microstructural view. Journal of Geophysical Research 103, 12223–12237.

Vidale, J.E., Li, Y.-G., 2003. Damage to the shallow Landers fault from the nearby Hector Mine earthquake. Nature 421 (6822), 524–526.

Wilkins, S.J., Gross, M.R., 2002. Normal fault growth in layered rocks at Split Mountain, Utah: influence of mechanical stratigraphy on dip linkage, fault restriction and fault scaling. Journal of Structural Geology 24 (9), 1413–1429.

Withjack, M.O., Callaway, S., 2000. Active normal faulting beneath a salt layer; an experimental study of deformation patterns in the cover sequence. American Association of Petroleum Geologists Bulletin 84 (5), 627–651.

Withjack, M.O., Olson, J., Peterson, E., 1990. Experimental models of extensional forced folds. American Association of Petroleum Geologists Bulletin 74 (7), 1038–1054.

Wu, S., Groshong, R.H., 1991. Low-temperature deformation of sandstone, southern Appalachian fold-thrust belt. Geological Society of America Bulletin 103, 861–875.

Xia, K., Rosakis, A.J., Kanamori, H., 2004. Laboratory earthquakes: the Sub-Reileigh-to-Supershear rupture transition. Science 303, 1859–1861.

Zhang, S., Tullis, T.E., 1998. The effect of fault slip on permeability and permeability anisotropy in quartz gouge. Tectonophysics 295 (1-2), 41–52.